HYRDRODYNAMIC AND SEDIMENTARY RESPONSE TO TROPICAL STORM BILL IN THE GULF OF MEXICO AND CHRISTMAS BAY

A Thesis

by

KEVIN E. FROST

Submitted to the Office of Graduate and Professional Studies of
Texas A&M University
in partial fulfillment of the requirements for the degree of

MASTER OF SCIENCE

Chair of Committee,	James Kaihatu
Co-Chair of Committee	Jens Figlus
Committee Member,	Chris Houser
Head of Department,	Robin Autenrieth

December 2015

Major Subject: Ocean Engineering

ABSTRACT

Follet's Island is a sand starved barrier island along the Northern coast of Texas. Human interaction has provided this island with an extended history of erosion, with some estimates having the island be completely eroded in 100 years. Compounding the issue of erosion is the vulnerability to hurricanes, tropical storms, and cold fronts around Follet's Island. These large storms cause major morphologic changes and erosion to the areas directly hit and surrounding the storm, and Follet's Island has one of the shortest return periods in the country for Hurricanes and Tropical Storms.

Two instrumentation pods were deployed in the Gulf of Mexico and Christmas Bay along a transect which bisected Follet's Island, with each pod located approximately 800 m from the island. Each pod was equipped with an acoustic Doppler current profiler and optical backscatter sensor. During the deployment Tropical Storm Bill made landfall approximately 160 km southwest of the deployment allowing the pods to measure the hydrodynamics and suspended sediment concentrations in response to the storm. Maximum storm surge from the Gulf of Mexico and Christmas Bay pods were measured to be 0.81 m and 0.52 m, respectively. The maximum significant wave height recorded was 1.93 m in the Gulf of Mexico and 0.23 m in Christmas Bay compared to 0.15 and 0.03 m during calm conditions respectively. Maximum suspended sediment concentrations for both pods occurred after the storm had made landfall during the ebb of the storm surge. Suspended sediment concentration loads reached peaks of 8.59 g/L and 3.09 g/L for the offshore and back bay measurements, respectively.

The time averaged cross shore and longshore sediment transports were calculated using the current velocity components and the suspended sediment concentration. The long shore transport showed a net drift to the west corresponding with the ebb of the storm surge. The cross shore transport displayed a net drift towards the ocean side of the island for both pods.

DEDICATION

I would like to dedicate this thesis to my father, mother, and sister. Without all of your love and support I would never be where I am today. I truly thank each one of you for your enduring belief in my abilities. Thanks, I love y'all immensely.

ACKNOWLEDGEMENTS

I would like to acknowledge my adviser and committee co-chair Dr. Jens Figlus, your eternal optimism and steadfast support has helped me overcome the most difficult challenge of my life. I would also like to acknowledge my other advisors, chair of committee, Dr. James Kaihatu and committee member, Dr. Chris Houser. Thank you for all of your guidance and knowledge throughout this research. Thanks also to Dr. Tim Dellapenna for letting us use your kayaks and boat, and to Josh Williams for helping with the deployment and recovery.

Thanks also to my friends and colleagues that I have met in both Galveston and College Station. You all made my experience at Texas A&M extremely fun and memorable. This thesis was supported in part by an Institutional Grant (NA14OAR4170102) to the Texas Sea Grant College Program from the National Sea Grant Office, National Oceanic and Atmospheric Administration, U.S. Department of Commerce

NOMENCLATURE

ADCP	Acoustic Doppler Current Profiler
GEV	Generalized Extreme Value
MAB	Meters above the Bed
OBS	Optical Backscatter Sensor
SPR	Strategic Petroleum Reserve

TABLE OF CONTENTS

Page

LIST OF FIGURES

Page

LIST OF TABLES

Page

1. INTRODUCTION

1.1 Motivation

Ocean and back bay interaction around barrier islands during storms is poorly understood. Follet's Island, a sand starved barrier island on the northern Texas coastline, has been serving as a case study for Texas A&M University at Galveston. Previous and ongoing research on this island has included numerical modeling, sediment coring, and beach profile surveying. This project aims to measure the interaction between the Gulf of Mexico and Christmas Bay directly through field instrumentation deployments during a tropical storm.

The State of Texas is home to the 6th largest amount of coastline in the United States (Texas General Land Office 2015). This coastline serves as a valuable resource protecting costly Texas infrastructure from storms and waves. The upper Texas coast is especially vulnerable to storms as it has a short return period for tropical systems relative to the rest of the state (Keim et al. 2007). Human interaction has severely decreased sediment supply along much of the coastline (Texas General Land Office 2015, Watson 2003, and Anderson 2007). This has created serious long term erosion for much of the coastline (Paine et al. 2012).

The Strategic Petroleum Reserve is the largest federal oil reserve in the county. Located 3 miles Southwest of Freeport, TX is one of the four SPR facilities. Bryan Mound is capable of holding 254 million barrels of oil at maximum capacity on a 500 acre campus. Recently the price of oil has declined, but even at a conservative rate of $40 per barrel, Bryan Mound still holds $10 billion worth of oil. In 2008, this plant was damaged by Hurricane Ike causing it a 6 day recovery period and costing $4.8 million in repairs (U.S. Department of Energy 2008). Approximately 8 km from the oil reserve is a barrier island, Follet's Island, which acts as a primary line of defense against wave attacks and storm surge. Follet's Island has a long history of erosion and has nearly been destroyed once. Without a proper solution for long term sustainability, this barrier island and protection for not only the Bryan Mound, but also other valuable infrastructure,

including evacuation routes and coastal communities, as well as, ecosystems, including the Brazoria Natural Wildlife Refuge and Christmas Bay, could be destroyed by future storms.

Follet's Island has an extended history of human interaction which has altered the natural sediment flux and influenced the island morphology. Construction of the Freeport jetties, the rerouting of the Brazos river delta, and the construction of the Galveston groin system have significantly altered the natural littoral drift in the area. In 1896, construction was completed on the Freeport jetties to protect the Freeport harbor entrance channel. Originally, the Brazos delta was located in Freeport channel at the western end of Follet's Island (Figure 1.1). This delta supplied sediment to Follet's Island on a constant basis. Once the Freeport jetties were constructed, large amounts of accretion formed on the Northeast side of the Jetties. In 1929, the Brazos River was diverted to combat the large accretion that had formed, and the new river delta was placed 7 miles Southwest of Freeport. This rerouting had an immediate effect on the sediment budget for Follet's Island. The former delta quickly began eroding, as did the surrounding area of Follet's Island (Morton and Pieper 1975). The Galveston groin system was completed in 1967 (Watson 2003). This series of 15 groins along the east side of the island have reduced the supply of sediment to beaches to the Southwest (Watson 2003). Follet's Island is a sand starved barrier island (Morton and Piper 1975, Morton et al. 1995, Watson 2003, Wallace 2010). With no regular sediment supply, Follet's Island has been eroding for quite some time (Watson 2003). Erosion rates on Follet's Island have been estimated between 1.5 and 5.8 meters per year (Morton and Pieper 1975).

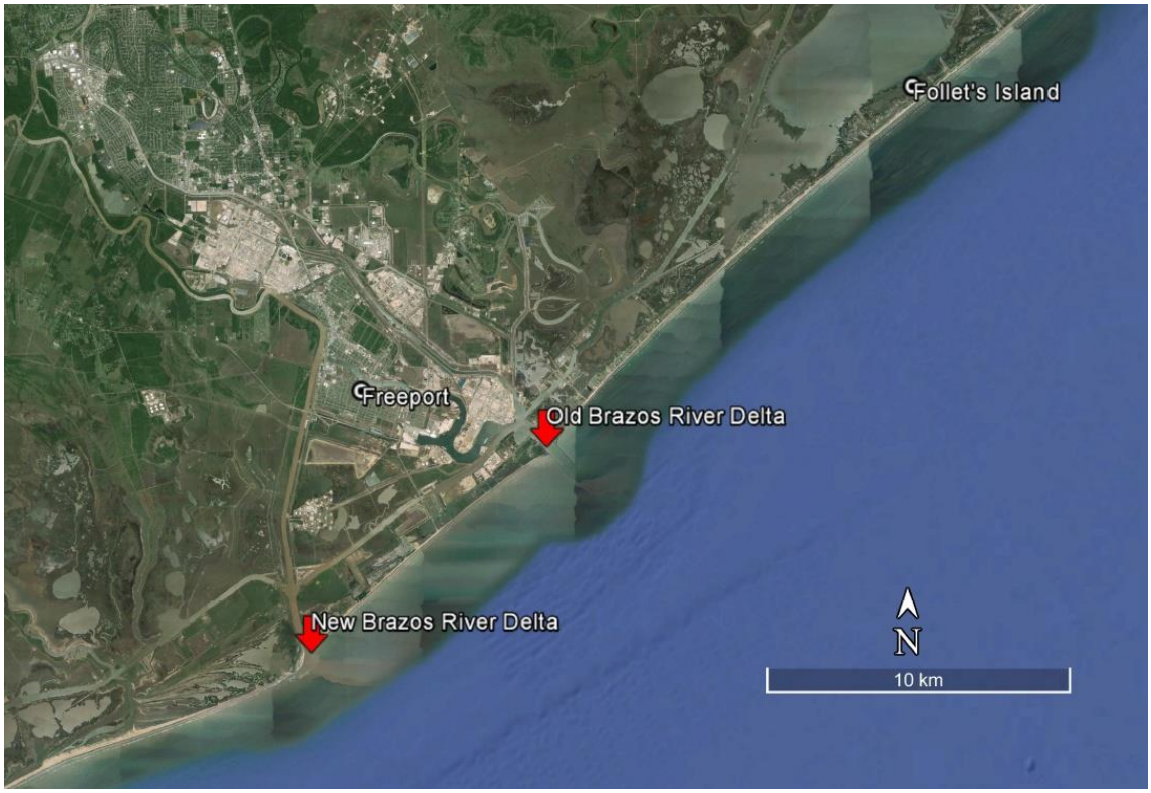

Figure 1.1 Relocation of the Brazos River Delta.
The Brazos River delta was diverted in 1929. This removed the natural sediment supply to Follet's Island thus, causing the island to be sand starved.

1.2 Objective

Originally, the aim of this project was to capture cold front dynamics in both the Gulf of Mexico and Christmas Bay as they strike on a much more consistent basis than tropical cyclones. Instrument pods were deployed during the summer of 2015 to measure baseline conditions between the two pods, however during this deployment Tropical Storm Bill quickly developed and made landfall near the instruments. This provided a very interesting data set depicting typical and storm conditions from field measurements.

This study aims to examine the interaction between the ocean and back bay of Follet's Island from storm forcing around Follet's Island. Many studies have suggested that barrier islands mitigate storm surge and wave attacks from the mainland, but this

would be the first study to measure this phenomena along the upper Texas coastline. Observing the storm dampening effects of barrier islands, as well as gaining an understanding of how storm forcing manipulates coastal sediments, can give an understanding of how to better engineer coastal developments in the future.

Two instrument pods measuring hydrodynamic and sedimentary response of the Gulf of Mexico and Christmas Bay along a transect which bisects Follet's Island during Tropical Storm Bill were deployed for a month and successfully recovered to obtain this dataset. By observing the currents movements, waves, and suspended sediment concentrations around the island, the interaction between the ocean and bay can be observed. This dataset also quantifies the protective properties which barrier islands have been reported to demonstrate.

This work is one of the first to quantify littoral drift around Follet's Island during a tropical storm. This project aims to better understand the relative importance of barrier protection along the upper Texas coastline. By understanding how barrier islands respond to tropical storms future coastal development can be bolstered by preventing human interaction from acting against natural processes.

1.3 Organization

This thesis is organized into five chapters. Chapter one gives a brief introduction to the project explaining the motivation, objective, and organization of the report. Chapter two presents a literature review on the history of the project location and surrounding area, pervious research on sediment transport during summer storms, and finally a description of Tropical Storm Bill. Chapter three describes data acquisition and methods used for analysis. Chapter four provides results of the analysis. Chapter five discusses the results obtained and concludes the report.

2. LITERATURE REVIEW

2.1 Upper Texas Coastline

The upper Texas coastline (Figure 2.1), Sabine Pass to the Brazos River discharge, is comprised of natural beaches and developed coasts located on barrier islands, deltaic headlands, and peninsulas (HDR 2014). Twenty thousand years ago, ice covered the vast majority of Canada and the Northern United States (Anderson 2007). At that time, the shoreline of East Texas was located 80 miles south of its current position. The present day coastline began developing approximately 18,000 years ago as large ice sheets began to melt creating sea level rise over the continental shelf migrating the shoreline landward (Anderson 2007). Approximately 5.3 ka, East Texas displayed a hightly irregular coast, but between 3 ka and 1 ka Galveston and the Bolivar Peninsula began to form (Rodriguez et al. 2004). The current coast has a mild slope and a very low elevation, making even moderate tides dangerous to coastal development (HDR 2014). Three dynamic barriers (Bolivar Peninsula, Galveston, and Follet's Island) define the upper Texas coast and have an extended history of shoreline change (Wallace et al. 2010). The coast of upper Texas is microtidal, with tidal ranges generally less than 1 meter (HDR 2014). However, the tidal range is variable and strongly influenced by seasonal meteorology (HDR 2014). This variation typically creates larger tides in the Spring and Fall and lower tides in the Summer and Winter (HDR 2014). The average dry beach width, the width of beach between the water line and dunes, along the upper Texas Coast is typically less than 30 meters (HDR 2014). Beyond the beach are poorly developed dunes, making the upper Texas coast, extremely vulnerable to over wash events from Tropical storms (HDR 2014). The relative sea level rise has been calculated at 4-8 mm/yr. This is much higher than the national average of ~1 mm/yr. Much of this of the difference can be attributed to subsidence of the Texas coast which has been measured at rates of 1-22 mm/yr (Paine 1993).

2.2 Barrier Islands

Barrier islands are narrow, long, deposits of sediment directly offshore of the mainland which run parallel to the coastline. These islands are separated from the mainland by bays, sounds, or lagoon and are generally found in chains along the East and Gulf coasts of the United States. Barrier islands compose approximately 80% of the Texas coast (Morton 1994). Hoyt (1967) gives the best explanation to the formation of barrier islands. This study discusses and rejects many of the previously accepted theories of barrier island formation such as development from offshore bars, emergent bars, and continuous development through the Holocene submergence. Hoyt (1967) states that barrier islands formed from the initial buildup of a ridge immediately landward of the shoreline from water and wind deposits. During the Holocene floods these areas experienced a slow submergence, and flooded the area landward of the ridge. This then created the barrier and bay system. After formation the island sediment supply and local hydrodynamics will control the migration of the island (Hoyt 1967).

Along the upper Texas coast, storm overwash will transport sediment from the ocean side of the island to the back barrier environment (Wallace et al. 2010). The barriers in this area are narrow, thin, and low lying allowing them to be overwashed easily (Morton 1994). These Barriers are retrogradational, thus are slowly retreating landward (Morton 1994). This is due to eroding deltaic headlands, cause by moving and inhibiting natural sediment supply to the area (Rodriguez et al. 2001).

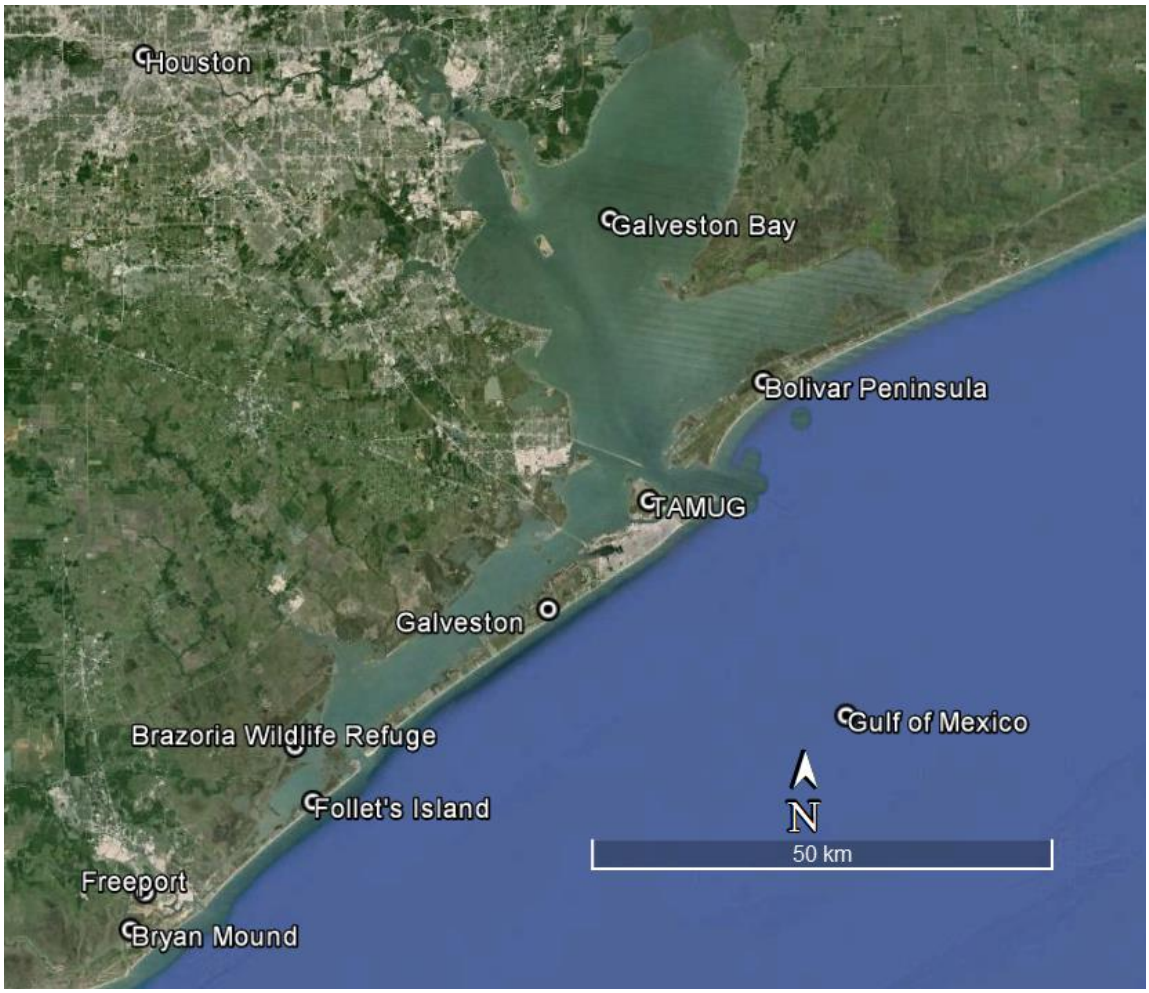

Figure 2.1 Upper Texas Coastline
The upper Texas coastline has a very low elevation and typically narrow beaches which protect the mainland from storms and wave attacks. This coastline is defined by three barriers: Bolivar Peninsula, Galveston, and Follet's Island.

2.3 Follet's Island

Follet's Island lies immediately to the West of Galveston Island on the Texas coast, and is the thinnest, most vulnerable stretch of coastline in Texas. The low lying island is, on average, between 0.23 and 0.45 km wide and has an average elevation approximately 1 m above sea level. Surrounding it are the Gulf of Mexico on the South, Christmas Bay to the North, the San Luis Pass and Galveston to the East, and Quintana to the West. Historically, Follet's Island has experienced serious coastal erosion and been damaged

by hurricanes. Numerous hurricanes, including Hurricane Carla, have completely submerged the island (Anderson 2007). Typically, waves and currents come from the South East, moving sediments in the South West direction (Morton et al. 1995).

Figure 2.2 Follet's Island
Follet's Island is a sand starved barrier island along the upper Texas coastline. This island has an extended history of erosion and has been extensively damaged by hurricanes in the past.

2.4 Sediment

The upper Texas coastline has a unique littoral drift at the expense of Follet's Island. Morton et al. (1995) states that there is an average southwestward littoral drift along the Northern Texas coastline, but occasional meteorological events can reverse the direction for periods of time. The net littoral drift to the southwest has been estimated to

be 45,000 m^3/yr (U.S. Army Corps of Engineers 1983). Downdrift sediment accretion for Follet's Island is non-continuous (Morton et al. 1995). Sand eroded from Galveston Island gets deposited in a sand flat at the end of the island. A large flood shoal is located between Galveston and Follet's Island on the landward side of the inlet. Sand used for the accretion of Follet's Island comes from the San Luis Pass, a stable tidal inlet which has maximum current velocities between 0.6 and 1 m/s during a typical tidal cycle and ultimately from the flood shoal. This dispersion of sand is event driven and inefficient. Offshore of the island there is only a thin layer of sand overlying the deltaic mud (Watson 2003).

Walker (2001) measured the effects of wind on water level and sediment transport during Tropical Storm Frances and Hurricane Georges. A gradual water level set-up was observed before the storm. During the storm the water level increased by over a meter. Pre-storm suspended sediment levels were more than seven times lower than concentrations during the storm. The suspended sediment concentration remained significantly higher than pre-storm conditions for days after the storm has passed. High levels of suspended sediment resulted from strong winds, due to wind-wave resuspension.

Dunes located on Follet's Island are small (Watson 2003). Because of this, during large wave events only a small amount of sand is available to be transported offshore, helping mitigate wave damage (Watson 2003). If this sediment is transported to the offshore clay zone, it will not be taken back to the beach (Watson 2003). Most of the sand that is eroded from Follet's Island washes over into Christmas Bay (Figure 2.3) (Anderson 2007). This is referred to as the 'rollover' stage of barrier evolution (Anderson 2007). This is the final stage before the barrier island is completely eroded (Anderson 2007). However, during very large storm events which cause overtopping and inundation of the island, the surge ebb flow transports the sediment offshore (Sallenger 2000).

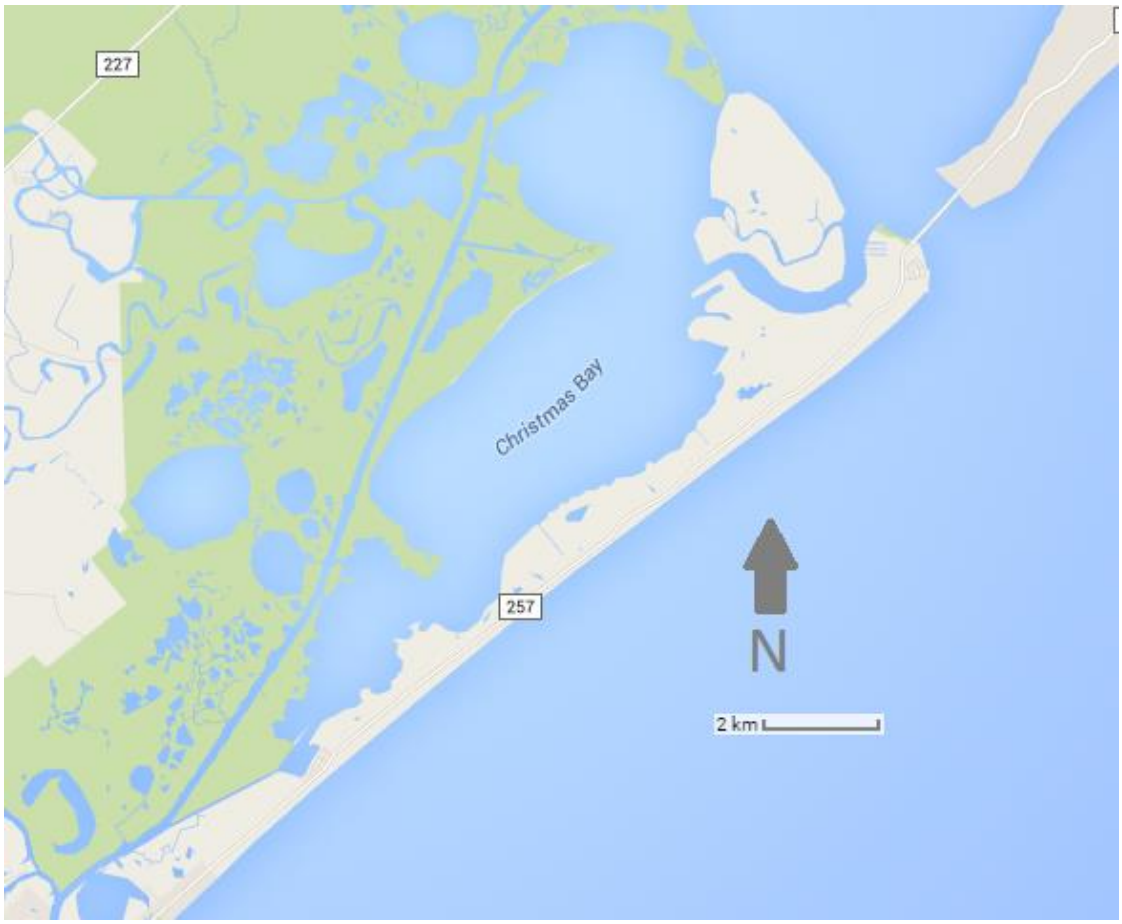

Figure 2.3 Christmas Bay
Christmas Bay separates the mainland of Texas from Follet's Island. Directly behind Christmas bay lies valuable ecosystems and infrastructure, including the Brazoria Wildlife Refuge and oil refineries.

Watson (2003) explains how the man-made changes northwest of Follet's Island have reduced the sediment transport down the Texas coast. Large quantities of sand are prevented from making their way down the coast due to the construction of Rollover Pass, the Bolivar Roads jetties, and the Galveston Groins (Watson 2003). Watson (2003) estimates that over 30 million cubic meters of sand has been permanently trapped because of these structures.

Sediment characteristics for Follet's Island have been described by Morton and Pieper (1975). The sediment ranges from mud or mud with a thin sand veneer, with high

concentrations of shell material, rock fragments, and caliche nodules, to predominantly sand with shell material (Morton and Pieper 1975). The sand fraction is well sorted fine to very fine sand and composed primarily of quartz (Morton and Pieper 1975). Shell content around Follet's Island ranges from 2 to 10 percent (Morton and Pieper 1975).

Due to their regularity cold fronts have been suggested to be the major driver in barrier island geomorphology on a year to year basis. However, tropical systems create more dramatic changes on an island in a short period (Roberts et. al 1987). Due to the costly infrastructure and inherent vulnerability, Follet's Island requires extensive examination.

2.5 Tropical Cyclone Exposure

The upper Texas coast has one of the shortest return periods for tropical storms and hurricanes in the Gulf of Mexico. Tropical storms are estimated to have a three year return period in the area, category 1-2 hurricanes have an eight year return period, and hurricanes category 3 and above have a 26 year return period (Keim et al. 2007). While the highest surge occurs where the storm makes landfall, areas near the storm will experience some extent of the storm surge as well. Figure 2.4 (Keim et al. 2007) depicts the return period for storms along the upper Texas coastline.

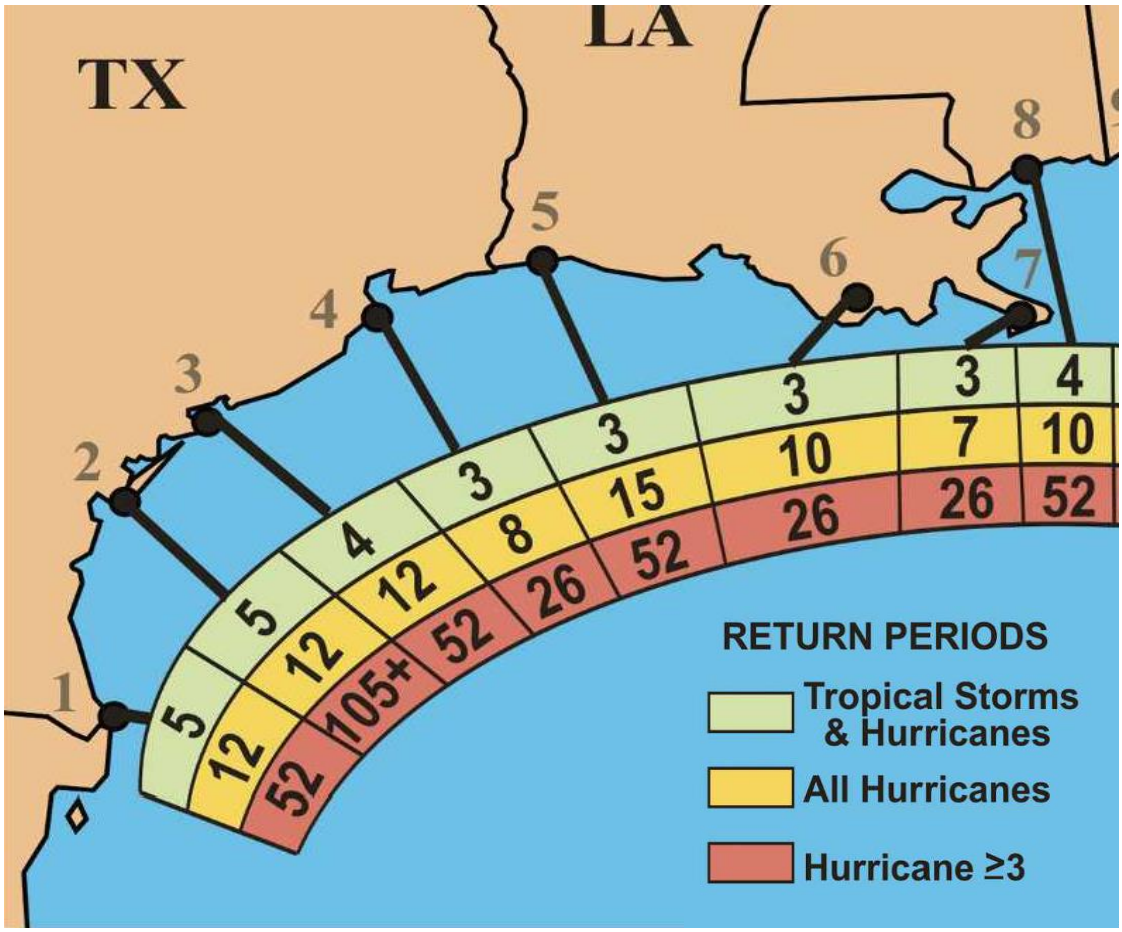

Figure 2.4 Regionalized Storm Return Period (Keim et al. 2007)
Follet's Island and the surrounding area (4) has one of the lowest return periods for Tropical Storms and Hurricanes in the nation.

Keim et al. (2007) also developed a Tropical Hazard Index (Figure 2.5) which quantifies an area's vulnerability to tropical cyclones. This number was calculated by assigning points to different types of tropical cyclone strikes to areas. A tropical storm are two points, category 1 and 2 hurricanes are four points, and a categories 3 and above are 8 points. This relative index provides an easy reference of storm frequency and intensity for coastal communities. Any location with a score over 100 denotes a

particularly vulnerable community. The Galveston area received a rating of 104, making it an exceptional location in terms of its storm vulnerability.

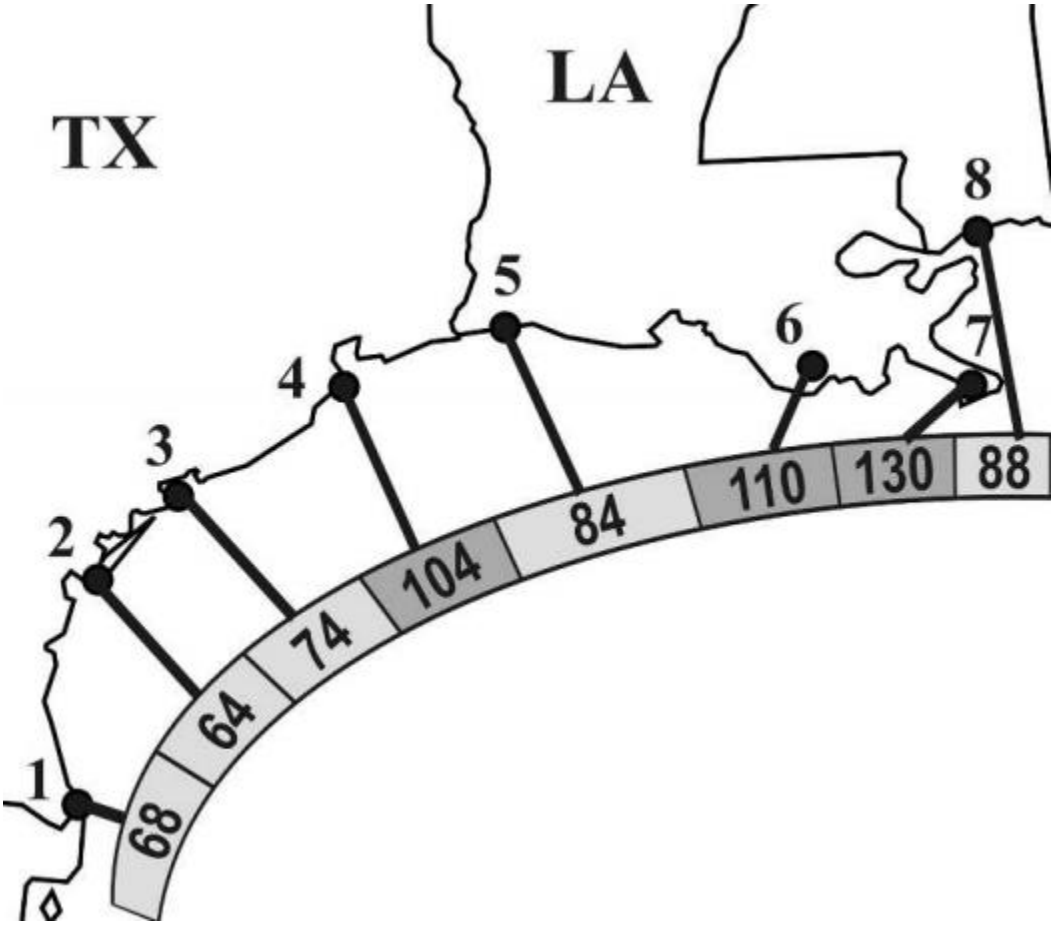

Figure 2.5 Tropical Hazard Index (Keim et al. 2007)
This figure depicts the tropical hazard index. This is a cumulative score for all of the tropical storms and hurricanes that have hit an area. Follet's Island and the surrounding area (4) have a score over 100 indicating that this area is extremely vulnerable to tropical storms and hurricanes.

2.6 Tropical Cyclone Response

Barrier islands play an integral role in protecting against erosion and flooding, as well as protecting vital ecosystems from storm forcing. Mainland erosion is mitigated with barrier island defense by the dampening effect that barrier islands have on wave climates (Stone and McBride 1998, List and Hansen 1992). Barrier islands take the brunt of the large waves generated by storms and only a small portion of the energy is still available to travel up inlets and refract around potentially complex geometry. Effective barriers lower storm surge vulnerability (Fritz el al. 2007). By acting as a natural dike barrier islands will lessen the storm surge effect on the mainland they protect. Finally, barrier islands protect wetlands, one of the earth's most valuable ecosystems (Van Heerden and DeRouen Jr. 1997). Wetlands have also been suggested to protect against storm surge (Costanza et al. 2008 and Wamsley et al. 2010). Without the barrier island, the wetlands behind it and the added defense against storms would be lost.

Barrier island suspended sediment concentration response to tropical cyclones, have been observed by numerous other studies. One of the earliest observations of the effects of tropical cyclones on barrier islands is Hayes (1967). This paper focused on hurricanes Carla (1961) and Cindy (1963). Hurricane Carla was an extremely large and destructive storm which made landfall over central Texas. Hurricane force winds were measured just North of Brownsville Texas and as East as Louisiana. Three environmental complexes affected by the storm were analyzed: the inner-neritic zone (0-120 feet depth), the barrier island complex and wind tidal flats. The inner-neritic zone undergoes large scale sediment transport as the storm surge ebbs. After the storm passes, strong currents flushed out of the numerous hurricane channels that were formed from the storm surge flood. These currents distributed a coarse sediment layer up to 3 cm thick over a previously homogenous mud to depths over 18 m. A turbidite layer up to 9 cm thick consisting of fine sand, silt, and clay, was placed even farther offshore (Hayes 1967).The barrier island complex endures drastic morphologic changes from storms. The beach was made longer and flatter from foredune erosion. Finally, the wind-tidal flats along the border of the barrier island were covered in a fresh layer of mud. This study

measured the largest suspended sediment concentration during the ebb of the storm as well, however the actual grain sizes for the transported sediment during this storm are unknown.

Wright et al. (1970) observed that the amount of damage differs, depending on which side of the storm an area is affected by. He analyzed the effects of Hurricane Camille (1969) on the Breton-Chandeleur island chain and the eastern portion of the Mississippi River Delta. Hurricane Camille passed on the east side of the Mississippi River Delta. This paper explained that morphological changes to the barrier island were mostly due to high waves and storm surge currents. It was also noted that there were large changes in water level position based on the quadrant of the storm passing through the area. Lower intensity winds and storm surge was indicative of the decreased damage on the western side of the storm as opposed to the eastern side due circulatory nature of the storm wind directions (Wright et al. 1970). In this study, Follet's Island was located on the eastern side of the storm.

Sheremet et al (2004) measured waves and suspended sediment concentration on the muddy inner shelf of the Atachafalaya Basin, Louisiana during located on the eastern side of Hurricane Claudette (2003). The study area was composed of fine silt with a mean grain size of 6.71 μm. Suspended sediment concentration was measured with three OBS situated at 1, 2, and 3 m above the bed (MAB). Suspended sediment concentration at 1 MAB rose before the storm as the current velocity exceeded the critical speed for resuspension (30 cm/s). This study noticed that the highest suspended sediment concentrations were measured as the sediment was settling after the storm had passed and, lasted for approximately 18 hours before decreasing again. During this settling phase 2 and 3 mab measured very low suspended sediment concentration levels as wave energy and current speeds had dissipated after the storm had passed. For this study only one optical backscatter sensor was used to measure sediment concentrations near the bed and, Suspended sediment concentrations remained above normal level for approximately 48 hours after the storm had made landfall.

2.7 Tropical Storm Bill

Tropical Storm Bill made landfall at 11:45 AM CDT on June 16, 2015 on Matagorda Island, less than 130 km from Follet's Island (Wiltgen et. al 2015). On June 12 the National Hurricane Center first noted a potential tropical cyclone formation in the Gulf of Mexico just North of Honduras. At this time the National Hurricane center predicted a low probability of the storm developing as the atmospheric conditions were unfavorable (Blake and Franklin 2015). The system then progressed to the northwest over the Yucatan Peninsula, and the chances for development increased as the storm moved back into the Gulf of Mexico (Cangialosi and Blake 2015). On June 14, the Air Force Reserve Hurricane Hunters began investigating the storm, and noticed a large area of low pressure had formed and tropical storm force winds were measured to the north and north east of the low pressure (Brennan 2015). The National Hurricane Center released the first public advisory for Tropical Storm Bill at 1:00 PM CDT leaving less than 24 hours for residents to prepare. Tropical Storm Bill reached maximum intensity at 10:00 AM CDT. At this time Bill had sustained wind speeds of 26.8 m/s and a minimum barometric pressure of 997 hPa (Wiltgen et. al 2015). Twenty eight centimeters of rainfall was measured in El Campo Texas from the tropical storm (Wiltgen et. al 2015). Storm surge was measured at 1.1m above normal tide level. Bill was downgraded to a tropical depression on June 17 at 4:00 PM CDT and continued to deteriorate over the next few days as the storm progressed to the northeast across the United States (Beven 2015). Figure 2.6 depicts the path of Tropical Storm Bill. Colored shapes along the path provide information about the storm classification and intensity at that point. Triangles represent a tropical depression classification. Circles represent tropical storm classification. Lighter shades of blue signify higher wind speed intensity.

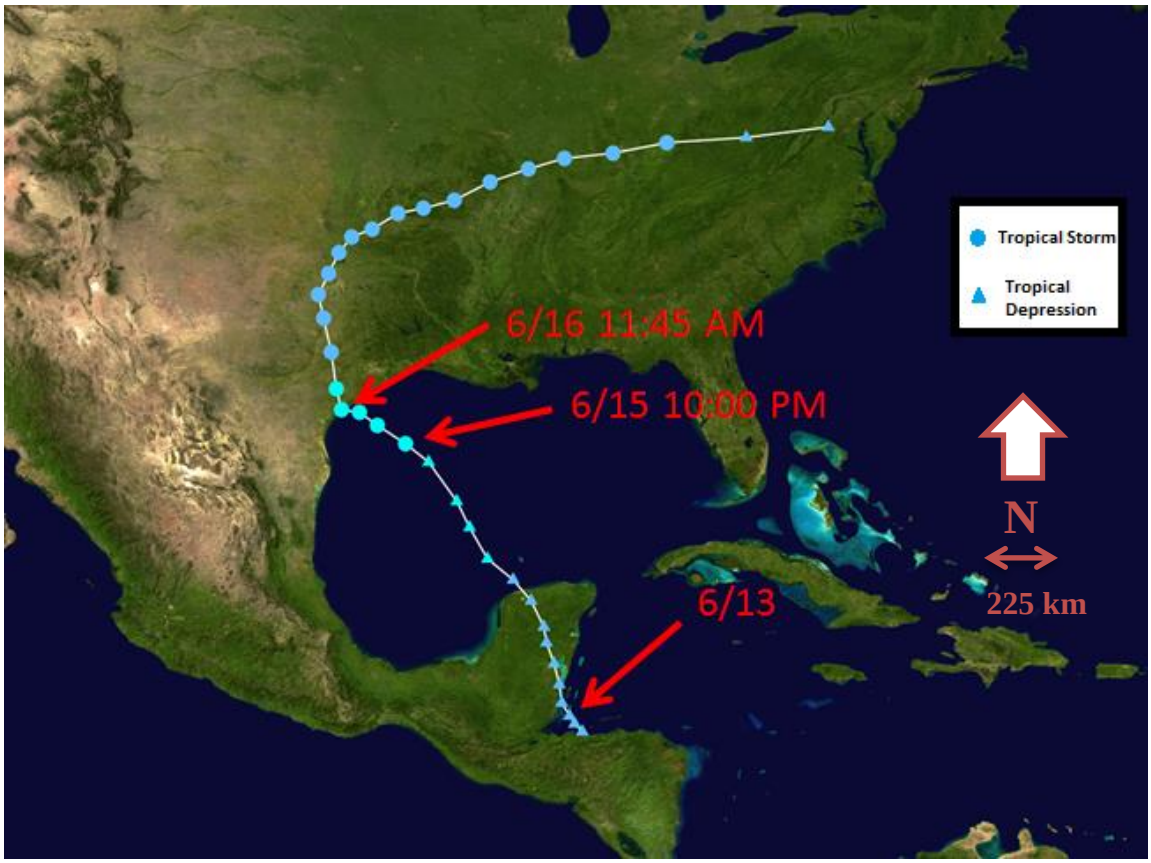

Figure 2.6 Path of Tropical Storm Bill
Tropical Storm Bill first began its development north of Honduras on June 12. It was declared a Tropical Storm on June 15 before making landfall the next day. In this figure the triangles represent a tropical depression, and circles represent a tropical storm classification.

3. DATA ACQUISITION AND METHODS

This chapter explains how data for this project was acquired and analyzed and is separated into two parts. The first section describes the instrument deployment and recovery explaining in detail the experiment setup, the theory behind the various instruments, and the location of the two sites.

Data analysis for this project was two-fold. Historic extrema analysis was developed for the area using wind, wave height, and storm surge data. The data acquired from the pods was then compared to the return periods calculated in an attempt to categorize the forcing mechanisms Tropical Storm Bill exerted on the two bodies of water. The second part of the data analysis was comparing the forcing mechanisms measured in the Gulf of Mexico and Christmas Bay in an attempt to observe the relative importance of barrier and back bay protection, as well as local sediment transport

3.1 Instrument Deployment

Two instrument pods were deployed around Follet's Island. The pods monitored waves, currents, tides, and sediment suspension from June 10, 2015 until June 26, 2015 to quantify sediment transport offshore and in the back bay. This chapter details the experiment design, calibration, deployment, and recovery.

Two instrumentation pods were designed to monitor waves, currents, tides, and sediment suspension concentration (Figure 3.1). Each pod was equipped with a Nortek Aquadopp HR profiler and an optical backscatter sensor. Both instruments on each pod were oriented to measure upward in the water column. The two devices were mounted on an aluminum frame with hose clamps and zip ties. An acoustic pinger (not pictured) was mounted on each of the pods on the handle opposite of the Aquadopp and OBS sensor heads to prevent interference.

Figure 3.1 Instrument Pod
One of these instrument pods was placed both in the Gulf of Mexico and Christmas Bay to sample simultaneously. These pods each contained a Nortek Aquadopp HR current profiler and an optical backscatter sensor.

The Nortek Aquadopp HR Profiler was used to monitor waves, currents, and tides. This instrument is a pulse coherent profiler which uses three acoustic beams to measure 3-d velocity profiles throughout the water column at predetermined bins. Sound pulses are transmitted from the instrument at a constant frequency and reflect off of particulate matter as the sound wave will not reflect off water alone. Plankton, sediment, and bubbles are good particulates which will reflect the sound wave. The instrument then ‘listens’ for the echo and separates the return signal in to different sections to process independently. After separating the second pulse, the phase difference between

to the two backscattered signals is calculated for each profile bin. Current velocity can then be directly measured by the phase difference using the following equation:

$$V = \frac{\Delta\varphi C}{4\pi f_{Source}\Delta t} \quad (1)$$

Where, V is the current velocity, $\Delta\varphi$ is the phase difference, f_{Source} is the transmitted frequency, and Δt is the time difference between two consecutive pulses. To compute the phase shift, the instrument measures the complex covariance between the two return pulses, then calculates the arctangent of the real and imaginary parts of the covariance function. The shorter lags in between pulses allow measurements of higher maximum velocity. Inversely, and more importantly for this study, longer lags (read: longer distances) have a lower maximum velocity that can be measured before phase wrapping will occur. As previously stated, the four quadrant arctangent function (atan2) is used to compute the phase shift between two consecutive pulses. The result of the arctangent function is confined to [-π, π]. Phase wrapping occurs when the measured the absolute value of the phase shift is greater ±π (Lohrmann et al., 1990 and Rusello et al., 2006).

Phase wrapping was encountered during Tropical Storm Bill due to the high velocities. This required an 'unwrapping' of the data. When phase wrapping occurs the recorded values will make a quick and large jump to the opposite sign. Therefore, to correct this issue these large jumps were located and changed by the following equation:

$$new\ velocity = old\ velocity\ \pm 2 * V_{amb} \quad (2)$$

Where, V_{amb} is the maximum velocity that the Aquadopp can measure.

The onboard liquid tilt sensor and magnetoresistive magnetometer records yaw, pitch, and roll for every velocity measurement to normalize the results into cardinal directions. The magnetometer measures each of the three components of the earth's magnetic field, and the liquid tilt sensor, measures the two tilt components and the up or down orientation of the head. The internal processing then synthesizes this information to compute the instrument's tilt and heading for each reading.

A silicone piezoresistive pressure sensor directly measures pressure on the Nortek Aquadopp HR. This device samples pressure once each second with a 1 mm

accuracy. However, there are known issues with the pressure sensor accuracy including long-term uncertainty, drift, resolution, and single-sample uncertainty. Long term drift in the pressure sensor is predominantly caused by temperature changes. The resolution and single-sample uncertainty are important when observing rapid changes in the free surface elevation, such as waves. For shallow sensors the resolution dominates this uncertainty.

Two different Aquadopp HRs were used for each deployment. A 1 MHz frequency Aquadopp was used for the offshore deployment and a 2 MHz Aquadopp was used for Christmas Bay. Since the Aquadopp processing will not record negative pressure, a 1 meter pressure offset was applied to the sensor as a safeguard against negative readings. The 'HR' or high resolution profiler included updated firmware which allows for sampling at scales smaller than 1 cm as fast as 8 Hz. Measurements are taken using a predetermined sampling scheme which can be seen in Appendix B.

For this deployment, the Aquadopp recorded in bursts for 1024 samples at 2 Hz every ten minutes. The Christmas Bay Aquadopp had a 0.096 m blanking distance and measured 12 bins spaced 3 cm apart. The offshore Aquadopp had a 0.4 m blanking distance and measured 19 bins spaced 10 cm apart. Figure 3.2 depicts the measuring scheme of the Aquadopp Profilers. This allowed for simultaneous sampling of pressure, velocity, and suspended sediment concentration across both pods. This scheme was decided upon to optimize the length of the deployment, since the instruments are battery limited.

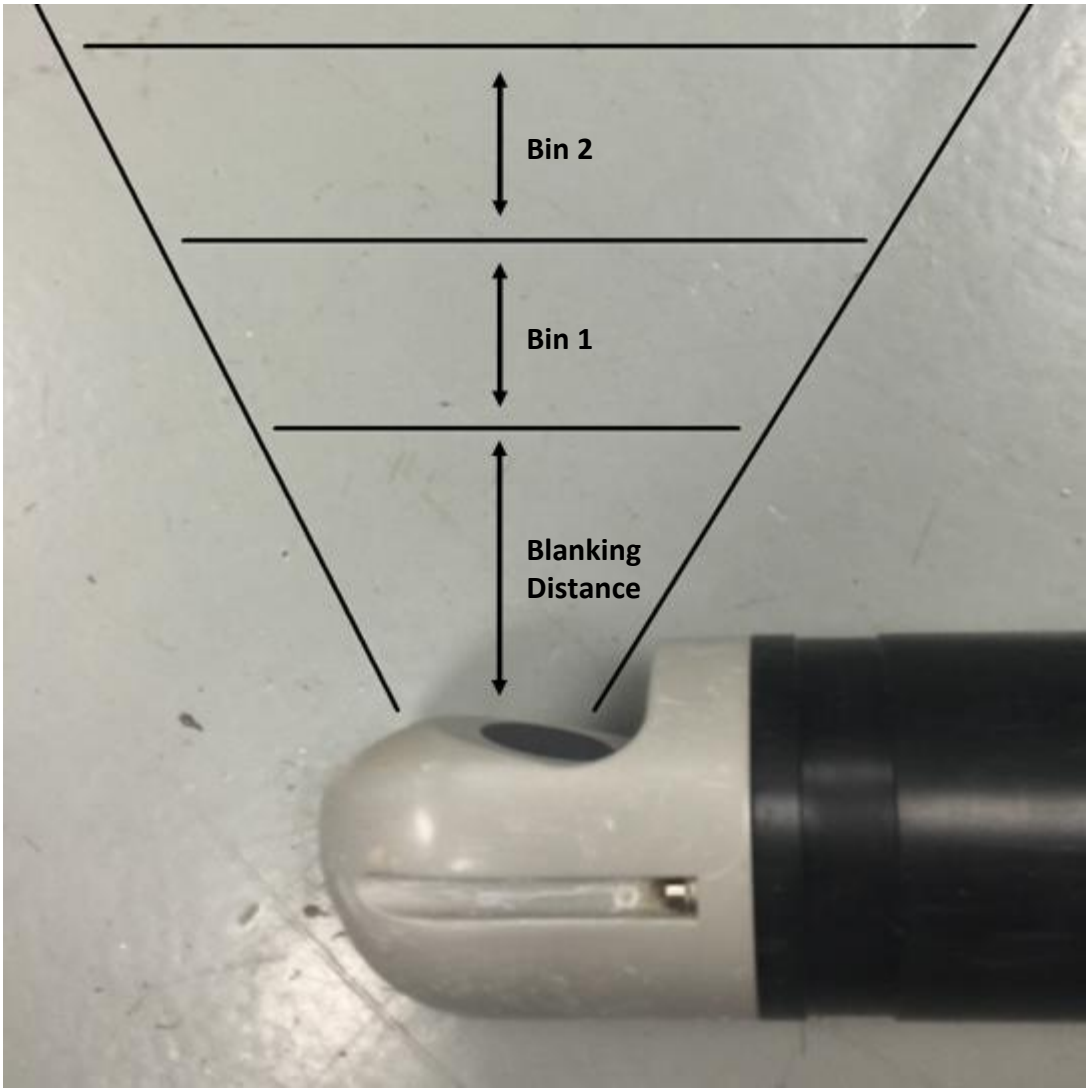

Figure 3.2 Aquadopp Measurement Scheme
Aquadopps measure currents throughout a water column as depicted above. Sound waves are produced by the head of the Aquadopp and reflect off of materials or bubbles in the water. The wave is then received back at the head where the velocity can be computed based on the distortion.

It is necessary to calibrate the onboard compass before deployment as different areas have different ambient magnetic fields. To calibrate the compasses the mounts, as they were deployed, were set up in a field away from other ferrous metals. The Aquadopps were then connected to a laptop with the Aquapro HR program installed.

The compass calibration function was chosen, and the device was slowly rotated around 360°. This process allows the device to accurately record heading information.

One Campbell Scientific OBS3+ (Figure 3.3)was mounted on each instrument pod. These devices measure suspended sediment concentration using reflected light. Light is sent out from the head of the device, and a voltage is recorded based on the amount of light that is reflected back to head. The OBS used power generated from the Aquadopp batteries and sampled simultaneously with the Aquadopp. This voltage can then be used to estimate suspended sediment at a point above the head by using calibration curves.

Figure 3.3 Campbell Scientific Optical Backscatter Sensor
The optical backscatter sensor uses light to estimate suspended sediment loads near the head of the device. This device produces light which is reflected and measured to give a voltage output. This voltage can be correlated to a suspended sediment concentration.

Acoustic pingers were mounted on each instrument pod to assist with the recovery. JW Fisher acoustic pingers (Figure 3.4) were used in an effort to ‘hear’ where the instrument was located on recovery. Once at the recorded GPS location of the instrument, a directional hydrophone was placed into the water to listen for the acoustic signal or ‘ping’ sent from the pinger. By rotating the hydrophone, the sound would get louder when pointed in the direction of the pinger, and softer when pointed away. This assisted in giving the recovery team a heading in relation to the boat when diving into the water.

Figure 3.4 Acoustic Pinger
Acoustic pingers are used to assist in locating deployed instruments. These devices emit sound at a known frequency which can be heard using a hydrophone.

The instrument pod mount used was built entirely out of Aluminum. Using a non-ferromagnetic material helped to reduce magnetic compass error. The base of the

mount was two rectangular bars 1.83m in length which connected together at their midpoints to create a cross. Large spikes (0.46 m long) were attached to the end of each bar of the cross. These spikes were designed to prevent sinking in the bay side deployment. The Aquadopp was mounted in a U-channel which was held above the mount by two 90 degree angle columns.

One design flaw from the mount was noted for future deployments. The cord which connects the battery canister and the Aquadopp had to be run through the handle of the mount. The cable must be removed from the Aquadopp and fed through the handle to remove the battery canister from the mount. This required all instruments to be dry before removing them from the mounts to prevent damage to any electronics. Cutting channel in the handle which the cord needs to run through would allow for removal of the instruments while they are still damp.

Two points were chosen to deploy instrumentation around Follet's Island (Figure 3.5). The locations were chosen based on a previous beach profile survey line. The instrument pods were installed offshore of the island and in Christmas Bay. The transect line made was determined by the Christmas Bay Deployment. Both pods were approximately 800 meters from the shoreline. The offshore pod was placed in 5 meters of water, and the Christmas Bay pod was in 1 meter of water. Once installed the heads of the Aquadopps were 47 cm and 26.5 cm above the bed for the offshore and bay deployments, respectively. The bay pod was lower because the sediment was easier to penetrate and completely anchor the mount spikes into the sand, whereas the offshore sediment was much harder and the divers were not able to penetrate the spikes fully. The OBS sensors were located 1 cm above the Aquadopp heads on both mounts due to the mounting configuration`.

Figure 3.5 Pod Deployment Location
The instrument pods were deployed on both sides of Follet's Island. These locations were chosen due to navigation ease and a recent beach profile survey.

The pods were deployed on June 10, 2015. The Christmas Bay pod was deployed first, due to scheduling issues. Initially, the device was to be towed to the site using two kayaks tied together. Luckily a local fisherman, whose wife happened to be an Aggie, offered to take the research team to the deployment site using his boat. To benefit the Christmas Bay deployment even further, the fisherman's boat was equipped with a power pole anchoring system. This is an electronic anchoring pole which is extended into the seabed from the stern of the boat, preventing boat drift once anchored. The pod was then placed onto the seabed at the predetermined site and the mount spikes were fully secured into the mud. Actual deployment coordinates were logged into a GPS to assist with recovery.

A 25’ Parker dual engine boat was used for the offshore deployment. The boat and research team embarked form the Bridge Harbor Yacht Club in Freeport, TX. Two AAUS scientific divers were necessary for the offshore deployment. During the expedition the dive team was briefed on local conditions, positioning, and stationing methods. The spikes were to be forced into the seafloor as deep as possible, and the head of the Aquadopp was to point North. Once at the site and anchored, the pod was hoisted over the side of the vessel. Dive bags were used to assist in submerging the pod. GPS coordinates were logged as the device descended into the water. The divers also took grab samples of local sediment on the seabed. A copy of the Deployment Manual used for this project can be seen in Appendix C.

Recovery of the two pods occurred on two separate days. The Christmas Bay pod was recovered on July 7, 2015. Unfortunately for the recovery efforts, there was no fisherman to offer their assistance. Three kayaks were used for the recovery. The first kayak contained a researcher and GPS in a ziplock bag to navigate to the site. The remaining two kayaks were tied together with a rope. The second researcher paddled in one of the kayaks while towing the other. Once near the site the research team tied themselves to the kayaks with ropes around their waists and dismounted from the vessels to search for the device while walking in the bay. The GPS lead the researchers directly to the pod. The pod was them lifted out of the water and placed on the kayak in tow. Due to strong currents, the instruments and kayaks had to be walked into shore.

The 25’ Parker was again used for recover the offshore pod. Because of energetic waves, the recovery of the offshore pod occurred on July 10, 2015, when conditions were safe. Again the boat embarked from the Bridge Harbor Yacht Club. Once at the site, coordinates the pinger receiver hydrophone was placed into the water. The pings were audibly louder when the hydrophone was pointed in the direction of the instrument pod, thus allowing the researchers to give the divers an initial heading to conduct search patterns.

To best estimate the suspended sediment concentration based on the voltage output from the OBS sensor, back calibration was necessary to create calibration curves.

Sediment samples collected at deployment were collected at each site to use for calibration. To calibrate the OBS methods from Pratt (1990) were used. The OBS was secured along the wall of the chamber with the sensing head pointed towards the center of the chamber (Figure 3.6) so that the walls of the chamber would not interfere with the recorded values. Measured concentrations mixtures of water and sediment were placed into a calibration chamber. A mixing device was placed into the calibration chamber to suspend the sediment. Once the sediment was observed to be in equilibrium voltage recordings from the OBS were taken for five minutes. An average recording was used to determine the voltage for that specific concentration. This was done for multiple concentration loads to ultimately create a calibration curve. Suspended sediment concentration was then calculated using the linear best fit line from the calibration curves. The readings were then averaged for each measurement burst, and a low pass filter of 10 minutes was used to remove spikes in the data that could have formed from any number of issues including, but not limited to, biota or sediment deposition on the sensor head.

Figure 3.6 OBS Calibration Chamber
This was the chamber used for OBS calibrations. Known amounts of sediment were added to a known amount of water and constantly mixed to keep the sediment in suspension. Average readings from 5 minutes of recordings were used for the calibration.

Sediment samples collected at each deployment location were run through a Malvern Mastersizer (Figure 3.7) to acquire grain size distribution and average grain size. This device is a laser diffraction particle size analyzer. This is done by measuring the angular variation of scattered light intensity as the laser scans particles that are fed through the device. Larger particles will scatter the laser at smaller angles than smaller particles. The particle size returned from the Mastersizer is an equivalent sphere diameter. Sediment density was also calculated by using a water displacement test on a known mass of each sample.

Figure 3.7 Malvern Mastersizer
The Malvern Mastersizer uses scattered light to determine the grain size distributions. The grab samples collected at each site were run though this machine.

3.2 Data Analysis

Data analysis for this project was two-fold. Historic extrema analysis was developed for the area using wind, wave height, and storm surge data. The data acquired from the pods were then compared to the return periods calculated in an attempt to categorize the forcing mechanisms Bill exerted on the two bodies of water. The second part in analysis was to compare the forcing mechanisms measured in the Gulf of Mexico and Christmas Bay in an attempt to observe the relative importance of barrier and back bay protection.

The cumulative moving average (Shumway and Stoffer 2002) is a smoothing function used in time series analysis. This function takes the average of the current values and the previous n values to remove noise of frequencies lower than the time

lapse of the n measurements. The cumulative moving average was a tool used in many analyses to remove or observe noise in data. The cumulative moving average equation was used for the low pass filters analysis:

$$CMA_n = \frac{x_{n-(n-1)} + x_{n-(n-2)} + \cdots + x_n}{n} \tag{3}$$

To categorize the magnitude of the storm surge generated by Tropical Storm Bill, an extrema analysis was performed on historic storm surge data located along the Texas coastline. Historical storm surge levels were gathered the SURGEDAT database maintained by Louisiana State University (Needham and Keim 2012). SURGEDAT is a comprehensive storm surge database which includes location and height of storm surge for 195 surge events as early as 1880 (Needham and Keim 2012). A storm surge return period plot was made using storm surge heights along the Texas coastline. A Log-Pearson Type III distribution was used for this analysis.

The Log Pearson Type III Distribution fits frequency distribution data to predict flooding (Oregon State University 2005). This distribution is recommended by the U.S. Water Advisory Committee on Water Data (1982) for flood frequency analysis. This distribution is calculated using the general equation:

$$\log(x) = \overline{\log(x)} + K\sigma_{\log(x)} \tag{4}$$

where, x is the flood value of some specified probability, $\overline{\log(x)}$ is the average of $\log(x)$, K is a function of the skewness coefficient and the return period. The values for K were found using a frequency factor table (Haan 1977). The mean is calculated by:

$$\overline{\log(x)} = \frac{\sum(\log(x_i))}{n} \tag{5}$$

The standard deviation is calculated by:

$$\sigma_{\log(x)} = \sqrt{\frac{\sum_i^n(\log(x) - \overline{\log(x)})^2}{n-1}} \tag{6}$$

Finally, the skewness coefficient is calculated by:

$$C_s = \frac{n\sum\left(\log(x) - \overline{\log(x)}\right)^3}{(n-1)(n-2)\left(\sigma_{\log(x)}\right)^3} \tag{7}$$

A recurrence interval chart was then used to interpolate for values of C_s and ultimately gain the return period table presented in the results.

A Gumbel distribution (Palutikof et al. 1999) was created to estimate wind speed return periods. Palutikof et al. (1999) stated that is long time series wind speed data are available then the Gumbel distribution will "almost certainly" be used. Twenty years of sustained wind speed data was acquired from the National Data Buoy Center. Annual maximum wind speed from stations 42035 and 42043 were chosen for this analysis due to their proximity to Follet's Island and their availability of historic wind data.

The Gumbel distribution as well as other Type I distributions are generally accepted as sufficient models for wind speed distribution. The Gumbel distribution is a parent distribution of the generalized extreme value (GEV) distribution. The probability density function for the GEV distribution is defined as:

$$F(x) = e^{-e^{-\frac{x-\beta}{\alpha}}} \tag{8}$$

where, β is the location parameter and α is the scale parameter. The cumulative probability for the GEV distribution is defined as:

$$F(X_T) = 1 - (\frac{1}{T}) \tag{9}$$

Where, X_T is the quantile, and T is the return period. Combining the PDF with the CDF for the GEV distribution and solving for X_T gives:

$$X_T = \beta - \alpha\, ln[-\ln\left(1 - \frac{1}{T}\right)] \tag{10}$$

To calculate the Gumbel distribution annual maximum are selected and ranked from the data set and applying the following equation derived from the GEV distribution probability density function:

$$y_{Gumbel} = -\ln\{-\ln[F(x)]\} \tag{11}$$

and:

$$F(x) = \frac{m}{N+1} \tag{12}$$

where, N is the number of observations, m is the numerical rank of the given observation and $F(x)$ is the probability that an annual maximum wind speed is less than the observation x.

Local wind speed and direction data was acquired from NDBC buoy 42043 for the course of the instrument deployment. Hourly maximum 8 minute averaged wind speeds were used to display maximum wind speed variations over the course of the deployment.

The Weibull distribution is a continuous probability distribution used for wave height return periods (Goda 1988). The probability distribution function for the Weibull distribution is defined as:

$$F(x) = 1 - e^{\left\{-\left[\frac{x-B}{A}\right]\right\}} \tag{13}$$

where, $F(x)$ is the probability of non-exceedance for the value x, A is the location parameter, and B is the scale parameter of the distribution. The reduced variate y is defined as:

$$y = \frac{x - B}{A} \tag{14}$$

The probability assigned to each value is a function of the ranking of the values and to determine their probability, $\widehat{F_m}$, using:

$$\widehat{F_m} = 1 - \frac{m - \alpha}{(N_T + \beta)} \tag{15}$$

Where, N_T is the number of extreme data points, m is the ranking in descending order from the largest value, and:

$$\alpha = 0.20 + \frac{0.27}{\sqrt{k}} \tag{16}$$

$$\beta = 0.20 + \frac{0.23}{\sqrt{k}} \tag{17}$$

A sensitivity analysis for values of $k = 0.75, 1, 1.4, 2$ was performed to create the best linear fit for:

$$x_R = \hat{A} y_r + \hat{B} \tag{18}$$

Where, $\hat{A}$ and $\hat{B}$ are the location and scale parameter estimates, respectively, x_R is the wave height for a given return period, and y_r is the reduced variate for a given return period calculated by:

$$y_R = [\ln(\lambda R)]^{\frac{1}{k}} \tag{19}$$

Where, λ is the ratio of extreme events per year for the dataset, and R is the return period.

The zero crossing method (Mizuguchi 1982) is a calculation for signal time series which takes the point where the sign of the function changes to estimate wave heights. The down crossing method uses the point where the sign of the function changes from positive to negative. This method was used to calculate wave heights by subtracting the minimum free surface elevation from the maximum free surface elevation in between two zero down crosses.

Welch's method is an estimate of the power of a signal at different frequencies used for computing power spectral density by sectioning the recorded data and averaging the modified periodograms of each (Welch 1967). This method uses the fast Fourier transform which decomposes a signal in time into the frequencies which make it up.

Let $X(j), j = 0, \dots, N-1$ be a stationary sample of a second order stochastic sequence with spectral density $P(f), f \leq \frac{1}{2}$. Segments of length L, which potentially overlap, are taken from the sequence, and the starting points of each segment is D units apart from the next. There are K segments, which cover the entirety of the record. A modified periodogram is calculated for each segment of length L, $W(j)$, and the finite Fourier transform is calculated for each segment window:

$$A_k(n) = \frac{1}{L}\sum_{n=0}^{L-1} x_k(j)W(j)e^{-2kijn/L} \tag{20}$$

Using this, K modified periodograms can be obtained:

$$I_k(f_n) = \frac{L}{U}|A_k(n)|^2 \qquad k = 1, 2, \dots, K \tag{21}$$

where,

$$f_n = \frac{n}{L} \qquad n = 0, \dots, \frac{L}{2} \tag{22}$$

and,

$$U = \frac{1}{L}\sum_{j=0}^{L-1} W^2(j) \tag{23}$$

Then the spectral estimate is the average of these periodograms:

$$\hat{P}(f_n) = \frac{1}{K}\sum_{k=1}^{K} I_k(f_n) \tag{24}$$

With this it is possible to show that:

$$E\{\hat{P}(f_n)\} = \int_{-\frac{1}{2}}^{\frac{1}{2}} h(f)P(f - f_n)df \tag{25}$$

where,

$$h(f) = \frac{1}{LU}\left|\sum_{j=0}^{L-1} W(j)e^{2\pi i f j}\right|^2 \tag{26}$$

and,

$$\int_{-\frac{1}{2}}^{\frac{1}{2}} h(f)df = 1 \tag{27}$$

A directional wave spectrum analysis was also performed by using DIWASP, a directional wave spectra toolbox for MATLAB which was developed by the university of Western Australia. This toolbox creates visualizations of directional wave spectrum based on pressure, u, and v velocity recordings (PUV method). Five different estimation methods are available with this toolbox, but the direct Fourier transform method (DFTM) was used for consistency with the non-directional wave spectrum analysis. The DFTM was developed using methods from Barber (1961). This is calculated by:

$$S_x(\omega) = \frac{1}{2\pi}\int_{-\infty}^{\infty} R_x(\tau)e^{-i\omega t}d\tau \tag{28}$$

where, $S_x(\omega)$ is the spectral density, ω is the angular frequency, $R_x(\tau)$ is th maximum values for the autocorrelation function of $x(t)$ with lag τ. The wave frequencies are then

associated with a direction based on the measured velocity. The DIWASP program produces a spectral matrix of evenly spaced frequencies and directions determined by the user.

Current velocity measurements were recorded by each Aquadopp. Current profiles were recorded based on the bin size and number. The reference frame of the recordings was taken with respect to the orientation of the Aquadopp in-situ. To normalize these values to an ENU (East North Up) coordinate system the following reference frame transformation was used.

$$\begin{Bmatrix} e_1 \\ e_2 \\ e_3 \end{Bmatrix} = \begin{bmatrix} cos\theta cos\psi & cos\theta sin\psi & -sin\theta \\ sin\phi sin\theta cos\psi - cos\phi sin\psi & sin\phi sin\theta sin\psi + cos\phi cos\psi & sin\phi cos\theta \\ cos\phi sin\theta cos\psi + sin\phi sin\psi & cos\phi sin\theta sin\psi - sin\phi cos\psi & cos\phi cos\theta \end{bmatrix} \begin{pmatrix} E_1 \\ E_2 \\ E_3 \end{pmatrix} \quad (29)$$

Where (E_1, E_2, E_3) is the original reference frame, ψ is the yaw, θ is the pitch, ϕ is the roll, and (e_1, e_2, e_3) is the transformed reference frame. The average yaw, pitch and roll were used to conserve computation time.

Only bins with an average correlation over 70% for the entirety of the time series were used to ensure measurement accuracy. Five bins were used from the offshore Aquadopp, and 10 bins were used from the Christmas Bay Aquadopp. Velocity readings were then depth averaged over the acceptable bins and a low pass filter of one hour was applied to observe trends in the dataset.

Bed stress (Dean and Dalrymple 2002) indicates the amount of shear stress placed on the water based on the roughness of the seafloor. Bed stress was calculated using the depth averaged velocity, drag coefficient, and the water density. The equation used for bed stress was:

$$\tau_b = \frac{1}{2}\rho C_d U^2 \quad (30)$$

Where, ρ is the density of seawater, C_d is the drag coefficient, and U is depth averaged burst averaged velocity. The drag coefficient and density were estimated to be 0.005 and 1020 kg/m^3 (Valle-Levinson et al. 2002), respectively.

The Shields parameter (Dean and Dalrymple 2002) is used as an indication of incipient motion. This dimensionless parameter is the ratio of shear forcing acting to mobilize sediment particles to the submerged weight of the particles. The equation for the Shields parameter is given as:

$$\Psi = \frac{\tau_b}{(\rho_s - \rho)gd} \tag{31}$$

where, Ψ is the Shields parameter, τ_b is the bed stress, ρ_s is the sediment density, ρ is the density of seawater, g is gravitational acceleration, and d is the mean grain size. If the Shields parameter is >0.03 then it is likely that the sediment particles will move. In the surf zone, breaking waves add a considerable amount of energy and turbulence into the water column, and sediment will mobilize at much lower velocities than predicted from the Shields parameter. However, the offshore pod was outside of the surf zone, and waves were not breaking in the bay.

4. RESULTS

This chapter presents the results of the historical data analysis, as well as the results of the pod deployment analysis. The intent of the historical data analysis is to quantify the forcing of Tropical Storm Bill in relation to various forcing constituent return periods. The intent of the pod deployment analysis is to quantify various forcing constituents at the two deployment locations, observe local hydrodynamics and to quantify sediment transport in the Gulf of Mexico and Christmas Bay.

4.1 Storm Surge

A storm surge return period distribution (Figure 4.1) was developed using a log-Pearson type III distribution and the SURGEDAT dataset (Needham and Keim 2012).

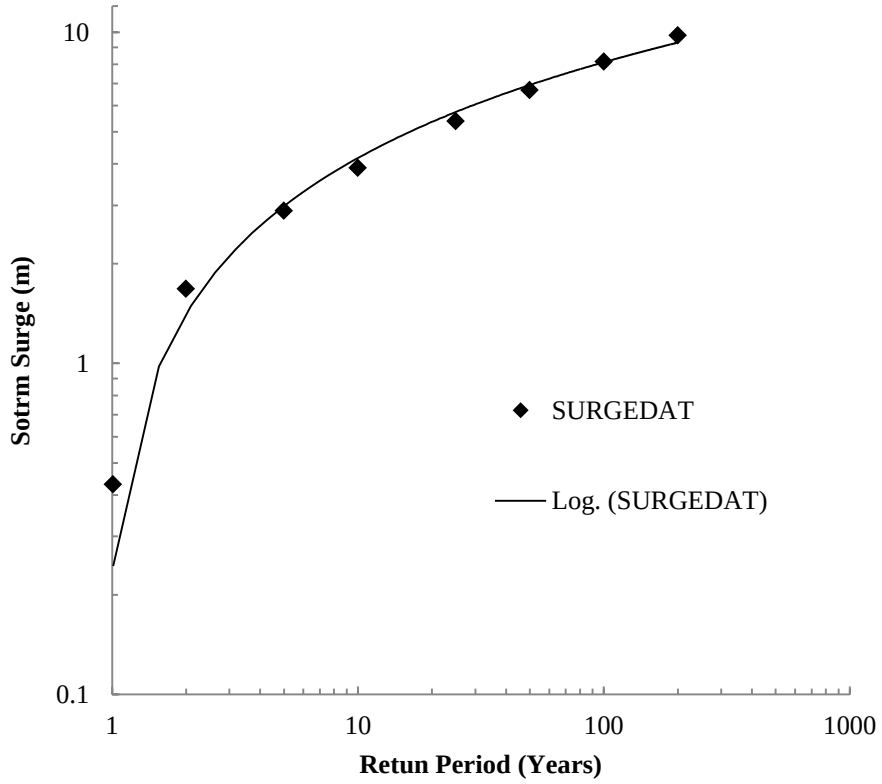

Figure 4.1 Log Pearson Type-III Storm Surge Return Period

Table 4.1 SURGEDAT Storm Surge Return Period

Return Period (Years)	Surge Height (m)
2	1.68
5	2.89
10	3.89
25	5.39
50	6.69

To observe tides and storm surge, the influence of waves needed to be removed from the pressure sensor readings. Low pass filters were used to observe both the tidal and storm surge influence, and solely the storm surge. A one day low pass filter was used to observe the storm surge. To observe the tidal influence the storm surge moving average was subtracted from a ten minute low pass filter that was applied to the original pressure data.

Depth measurements were taken by the Aquadopp pressure sensor. A one day moving average was applied to the depth recordings to observe storm surge (Figure 3). Upon recovery it was noticed that the offshore pod has settled into the bed approximately 20 cm. After reviewing the heading, pitch, and roll recordings of that device, it was surmised that there was a turbulent event which occurred on the 12th. Because of this storm surge measurements before this event were not used. A forerunner surge was evident from the increased water level 2 days before the storm hit. Forerunner surges are somewhat unique to the Louisiana and Texas coastline due to the wide and shallow shelf in the area (Kennedy et al. 2011). The maximum storm surge was measured at 0.81 m at the offshore pod and 0.52 m in the bay. After the storm had passed, there was still evidence of increased water level on both pods from the residing surge.

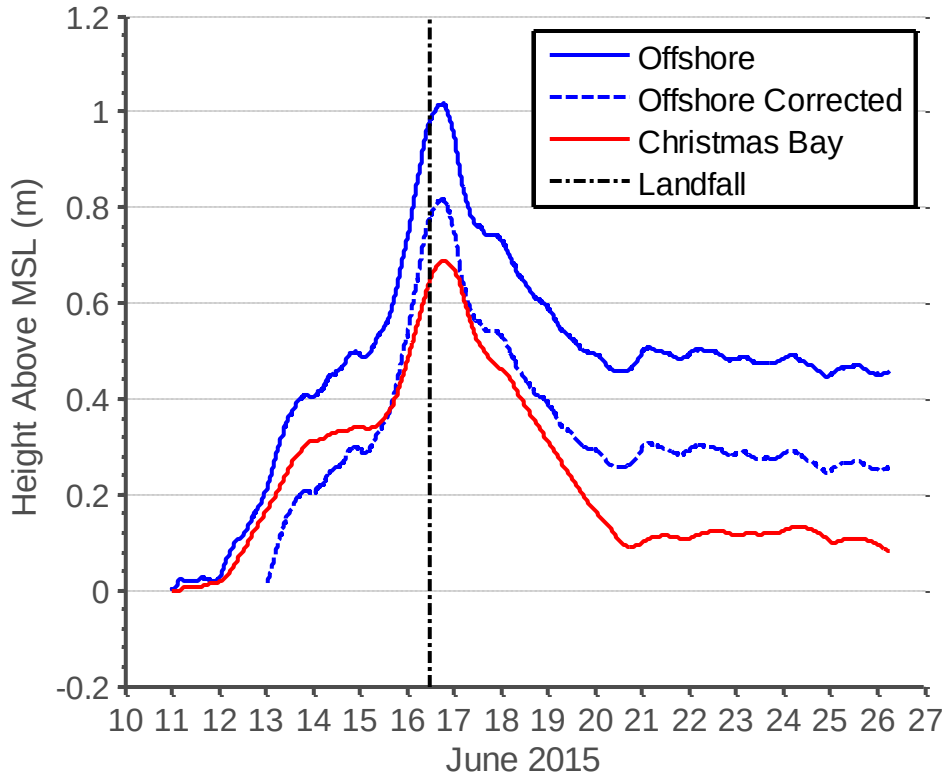

Figure 4.2 Storm Surge
Storm surge was calculated by removing the wind wave and tidal trends from the pressure data. The offshore corrected curve was added to account for the 20 cm drop which occurred on the 12th of June

Figure 4.3 displays the tidal fluctuation over the course of the deployment for each pod. Tidal fluctuations for the bay are smaller than that of the ocean due to the constriction of water being able to enter and exit the bay from the inlet and pass it is required to travel through. The largest tidal variations are associated with the passing of the storm.

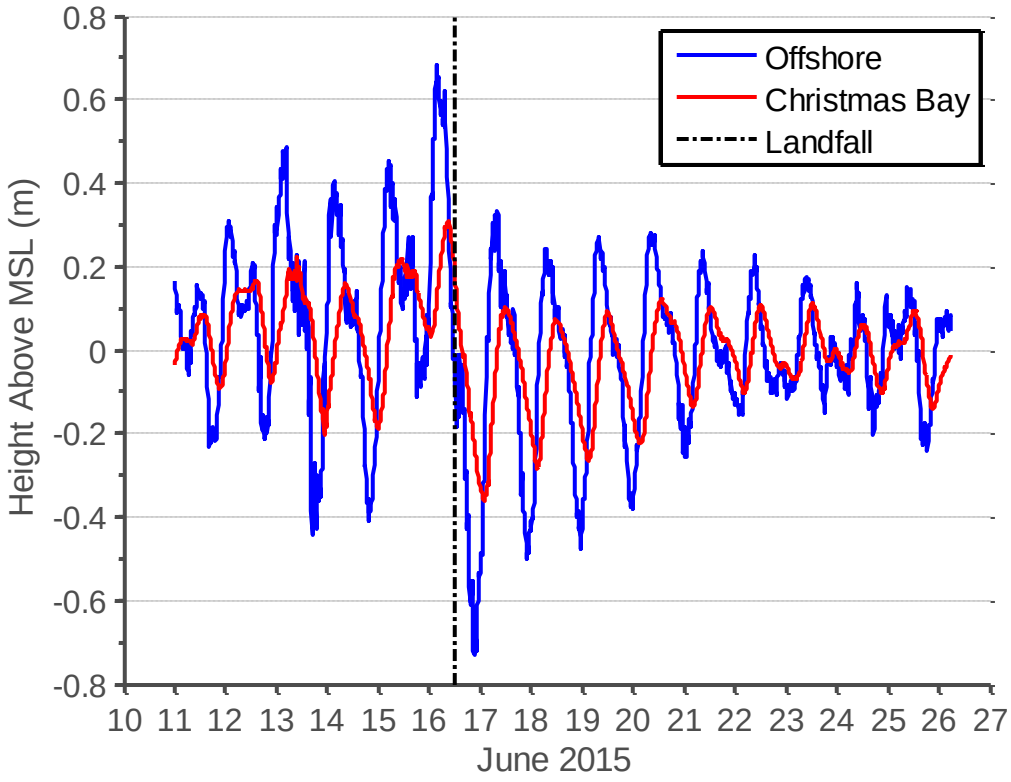

Figure 4.3 Tidal Fluctuation
Tidal fluctuations were larger in the Gulf of Mexico than in Christmas Bay. There is also a noticeable lag between the peak tides in both bodies of water.

4.2 Wind

Tropical Storm Bill had maximum recorded sustained winds of 13.8 m/s recorded at station 42035. This wind speed places bill between the two and three year return period. Buoy data for the duration of the deployment was acquired from Buoy 42043 which is maintained by the Texas A&M TABS system (Figure 4.4).

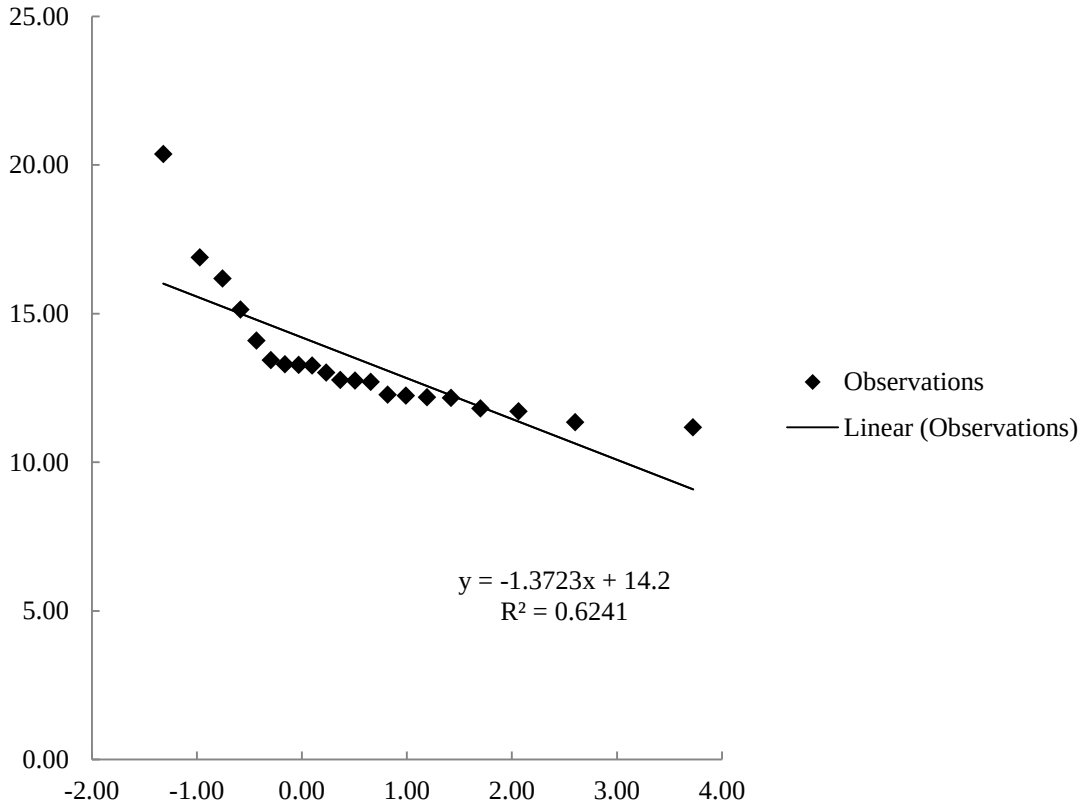

Figure 4.4 Wind Speed Return Period
This figure plots the wind speed (m/s) against the Gumbel reduced variate used in creating a yearly wind speed return period.

Table 4.2 Maximum Sustained Wind Speed Return Period

Return Period (Years)	Maximum Daily Wind Speed
2	13.09
3	14.02
5	15.06
10	16.36
25	18.01
50	19.23

Figure 4.5 depicts 8 minute sustained wind speeds at station 42043 and the wind direction. Wind direction is presented as the direction as which the wind is originating from. Predominant winds for the area are coming from the south and southeast. Average wind speed for the entire time series is 7.14 m/s. Before the storm (June 10-13) average wind speeds were 7.50 m/s. The wind direction during this time was predominantly from the south and southeast. Maximum wind speed was measured at 12.8 m/s on June 13 at 11:50 AM UTC. Minimum wind speed was measured at 2.6 m/s on June 10 at 12:50 PM UTC. This low speed occurred as the winds shifted and began blowing out of the northwest for a short portion of the day. On the days of the storm (June 15-17), average wind speed increased to 10.82 m/s. Maximum wind speed of 13.8 m/s was measured on June 16 at 11:50 PM UTC. The minimum wind speed during the storm was 7.9 m/s on June 15 at 3:50 UTC. Before and after landfall, the cyclical pattern of the tropical storm is evident as the wind is shifts from blowing west before the land fall to blowing north as the storm progressed over Texas.

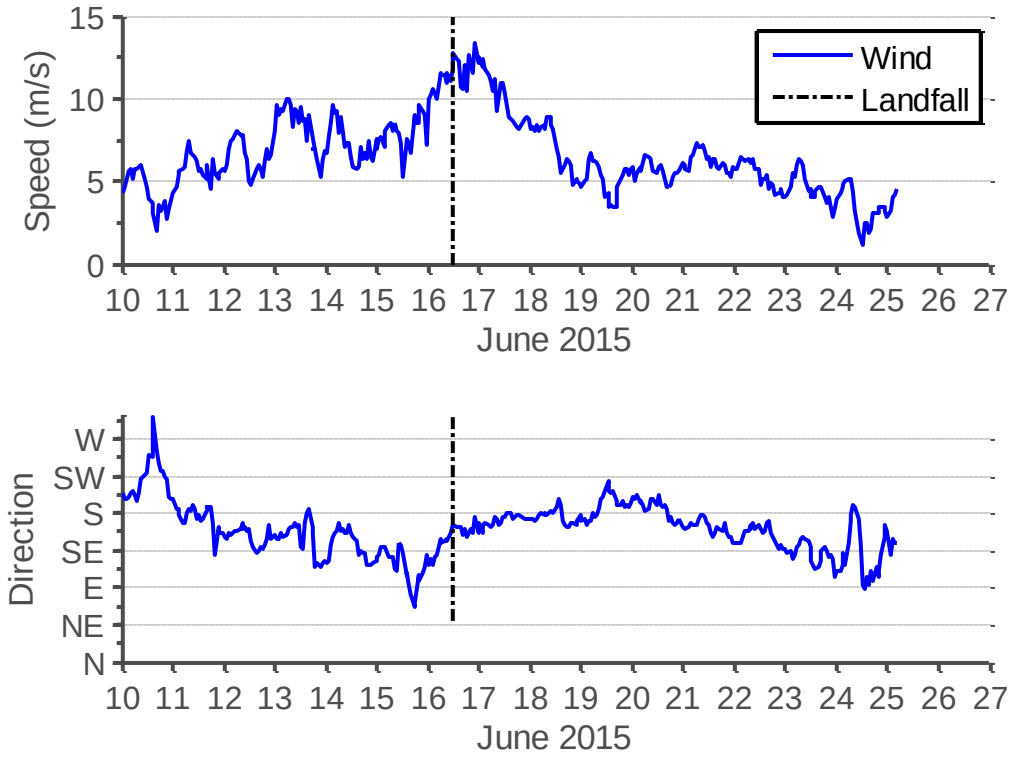

Figure 4.5 Wind Velocities
Wind velocities peaked at 13.8 m/s on June 16. The direction of the wind refers to the direction from which it is coming from.

4.3 Waves

Wave analysis from the deployment was calculated using pressure readings from the Aquadopp. To obtain the free surface elevation for wave analysis, a low pass filter 10 minute cumulative moving average was used on the pressure sensor recordings. This 10 minute moving average was then subtracted from the original dataset to observe free surface elevation changes. A zero down crossing method was then used to determine wave height. Significant wave height was determined by taking the mean of the largest one third of the waves in each sampling burst.

A Weibull Distribution was calculated using annual maximum wave height data over twenty years (Figure 4.6). A sensitivity analysis comparing the linear fit of the

maximum wave height and the Weibull reduced variate was preformed, and a value of $k = 1.0$ was used as it created the best fit for the regression. Average wave height offshore over 20 years is .88 m. Tropical Storm Bill created a maximum significant wave height of 2.9 meters at station 42035. This again places Tropical Storm Bill right on the five year return period (Table 4.3). Significant wave heights for both deployments were calculated by finding the average of the largest one third waves in each burst. The predominant wave period energy was found for each deployment using Welch's Method.

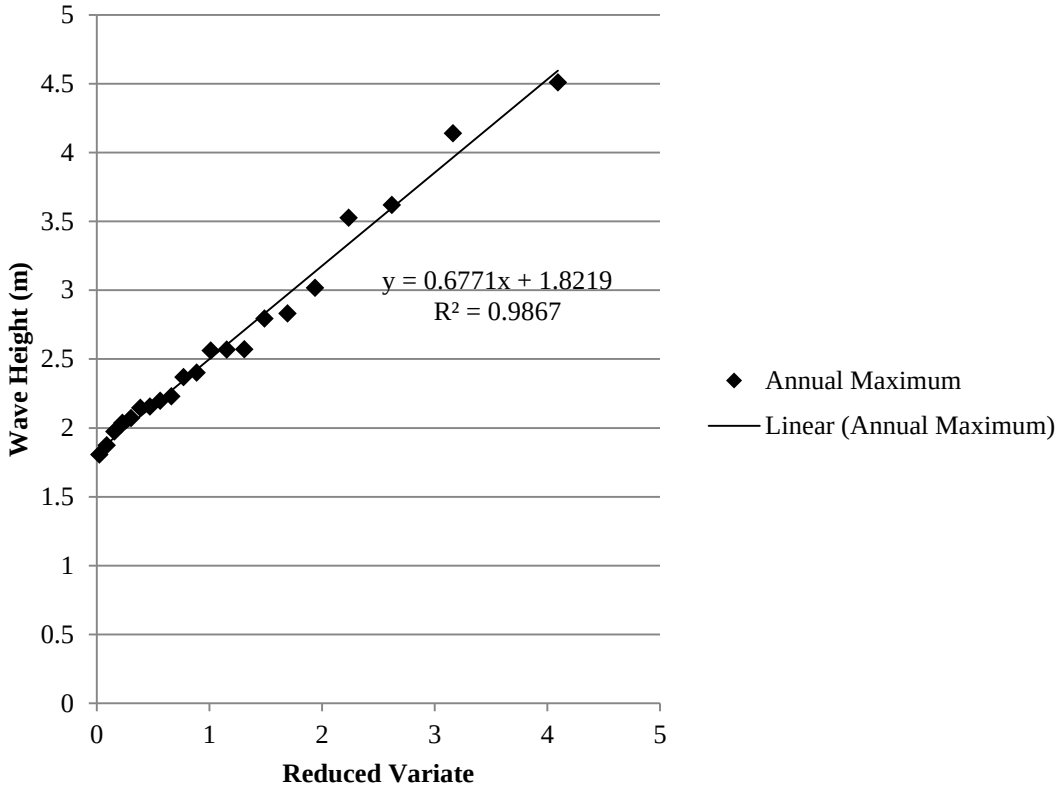

Figure 4.6 Wave Height Weibull Distribution
This figure plots the wave height (m) against the Weibull reduced variate used in creating a yearly wind speed return period.

Table 4.3 Wave Height Return Period

Return Period (Years)	Significant Wave Height (m)
2	2.28
3	2.55
5	2.90
10	3.36
25	3.97
50	4.43

A down crossing method was sued to convert the pressure data into free surface elevations. Figure 4.7 depicts a short envelope of the free surface elevation time series on the first day of measurements. At the time of deployment waves were very small waves offshore. When measurement stated on June 10 significant wave height was .1486 m corresponding with the low winds that came from onshore on that day. The significant wave height began to increase over the next day and displayed a peak of 0.44 m on June 11 at 11:10 PM. Wave heights continued to rise with the strong winds on the 12 and especially on the 13 reaching a maximum significant wave height of 1.49 m on June 13 at 3:00 AM UTC. Over the next day (June 14) wave heights decreased reaching a minimum of 0.63 m at 6:20 UTC during the calm before the storm. Wave heights then rapidly increased as the storm approached. During the 15 through the 17, the average significant wave height was 1.35 m. The maximum significant wave height recorded was 1.93 meters and occurred on June 16 at 9:30 AM UTC. After the storm made land fall the wave heights began to taper off and return to normal conditions. The average significant wave height from the 18 until the end of the time series was 0.40 m. The dominant wave period energy for the offshore deployment was 0.12 Hz or 8.33 s. Waves in Christmas Bay were a magnitude of difference smaller than the waves in the Gulf of Mexico and did not fluctuate nearly as much. From June 10 through the 14, the average significant wave height was 0.02 m. From the 15 to the 17, wave height increased but

only slightly. Average significant wave height during the storm was 0.06 m. Maximum measured significant wave height in the bay of 0.16 m occurred on the day of the storm at 3:30 PM UTC. After the storm passed, wave heights lowered and the average significant wave height was 0.02 m. Figure 4.8 depicts the significant wave height time series for both deployments.

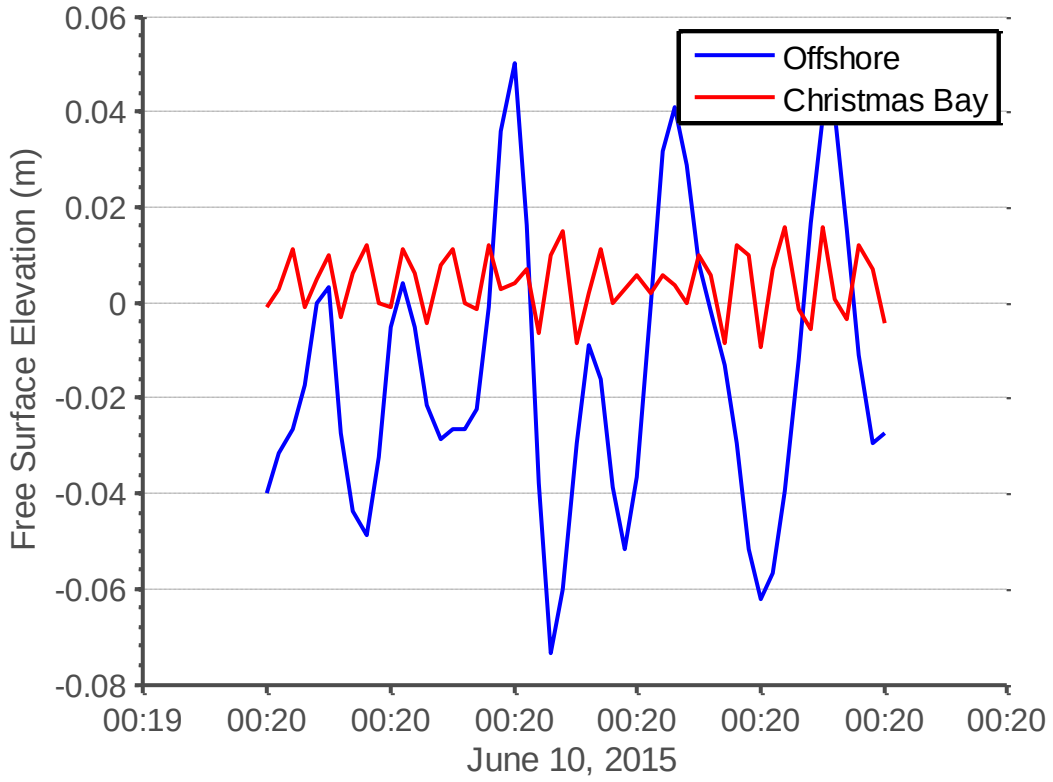

Figure 4.7 Free Surface Elevation Envelope
This is a small time series of the free surface elevation measured. Wave heights differed by at least an order of magnitude between the two pods.

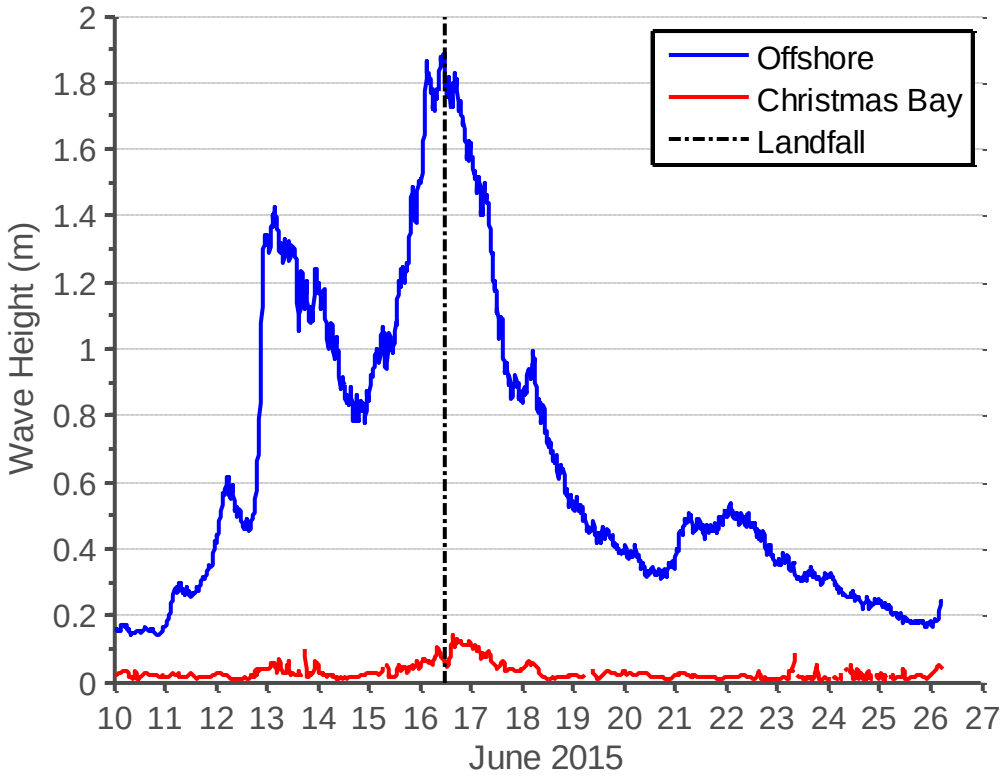

Figure 4.8 Significant Wave Height Time Series
The significant wave height peaked at 1.93 m on June 16 at the offshore pod. The maximum significant wave height in Christmas Bay was recorded at 0.16 m on the same day.

A wave energy spectrum was calculated for both deployments using Welch's Method (Figure 4.9). The dominant wave period energy for the Christmas Bay deployment was 0.45 Hz or 2.22 s.

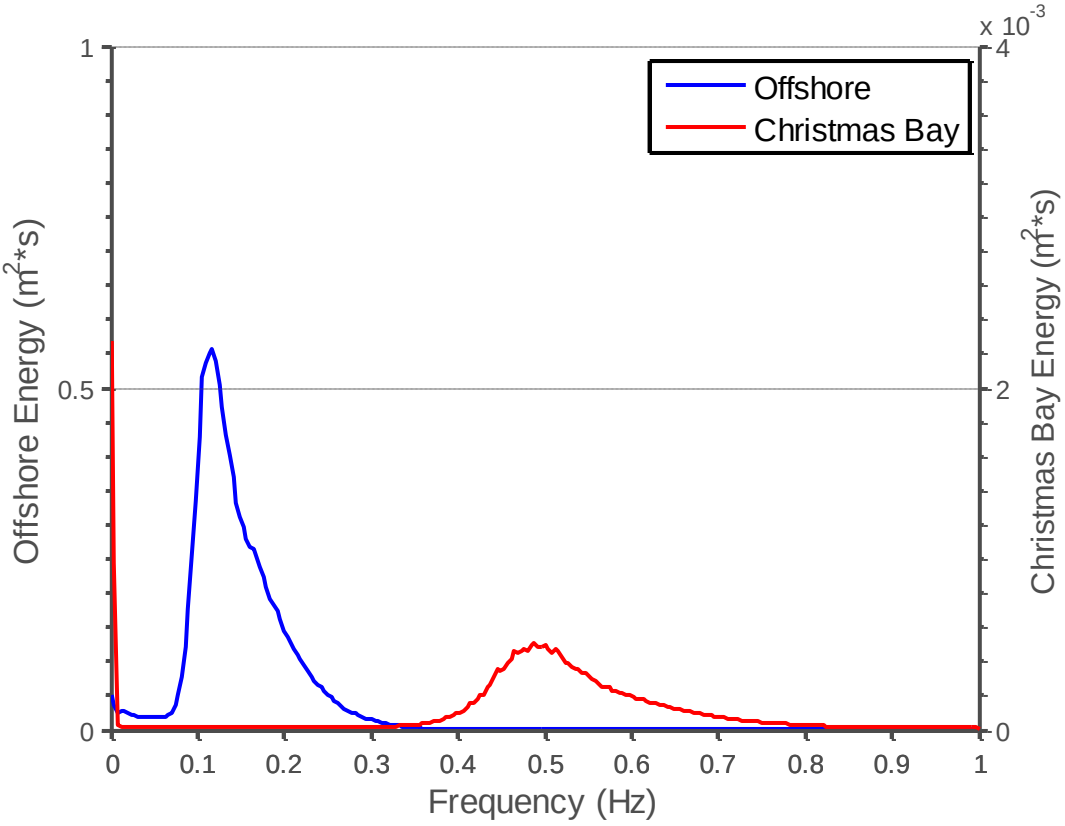

Figure 4.9 Power Spectral Density
The peak frequency for the offshore deployment was 8.33 s while the peak frequency for Christmas Bay was 2.22 s. There was also a difference in energy between the two pods of two orders of magnitude.

The directional wave spectrum was calculated using the PUV method from the previous section. For the PUV analysis the top acceptable bin from the velocity measurements was used. Figure 4.10 and Figure 4.11 display the calculated directional spectrum for the offshore and Christmas Bay deployment, respectively. The offshore deployment had a peak wave period of 8.33 second at 320° relative to North. When separating the directional wave spectrum by days, this was rather typical of all of the days of the deployment other than the day which Bill made landfall (June 16th). On that day the peak period was 9.09 s at 40° relative to North as seen in Figure 4.11.

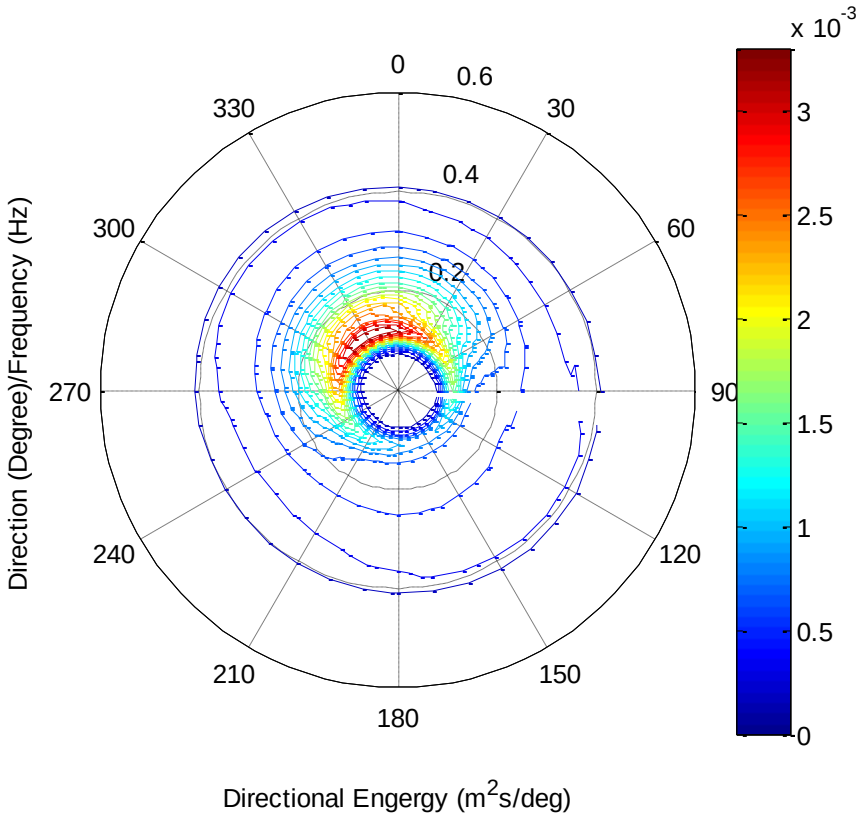

Figure 4.10 Offshore Directional Wave Spectrum
This figure depicts the directional wave spectrum in the Gulf of Mexico for the entirety of the time series. The peak direction of the waves was at 340° with a period of 8.33 s.

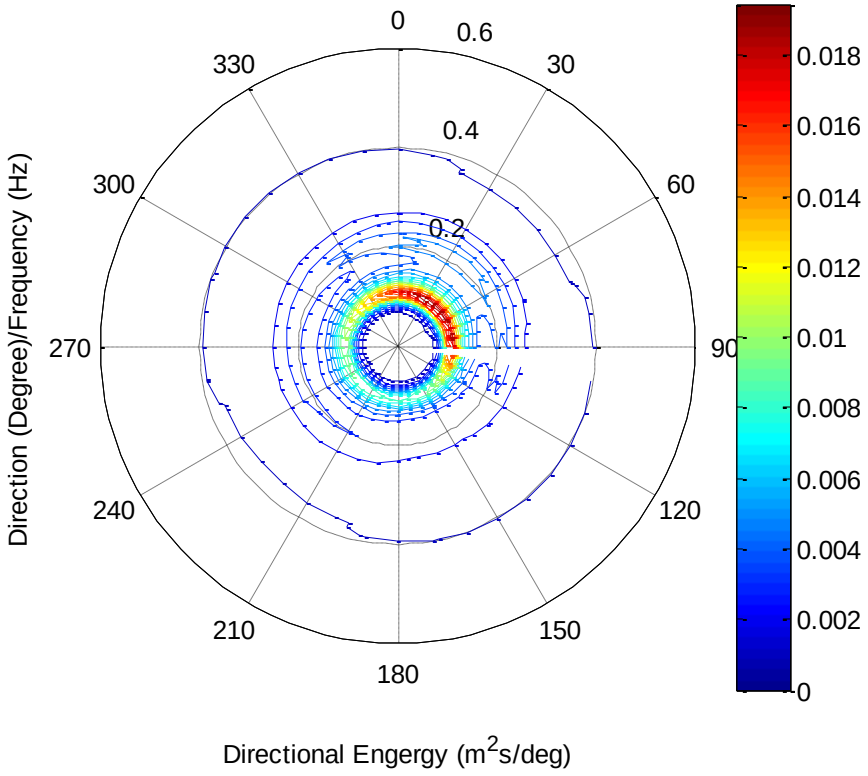

Figure 4.11 Offshore Directional Wave Spectrum During Tropical Storm Bill
This figure depicts the directional wave spectrum in Christmas Bay for June 16. The peak direction of the waves was at 40° with a period of 9.09 s.

The Christmas Bay directional wave spectrum displayed two dominant wave directions. The most dominant direction had a peak period of 2.04 s at 350° relative to North. The other dominant wave direction is at approximately 175° relative to North and this could be from wave reflection across the bay seen in figure 4.12. Tropical Storm Bill only caused the wave direction to shift slightly west. The predominant direction was at 340° with a dominant period of 2.13 s. The second dominant direction is visible again during the storm, and reflection can be assumed to create these lower energy waves.

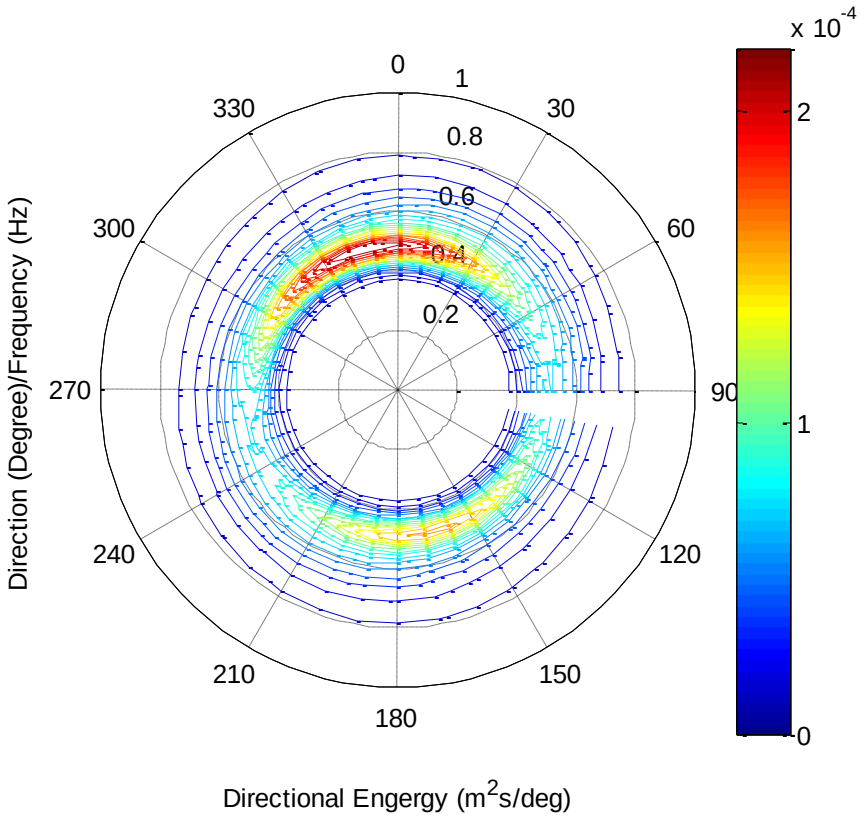

Figure 4.12 Christmas Bay Directional Wave Spectrum
This figure depicts the directional wave spectrum in Christmas Bay for the entirety of the time series. The peak direction of the waves was at 350° with a period of 2.04 s. The smaller mass of wave energy was from reflections of waves across the bay.

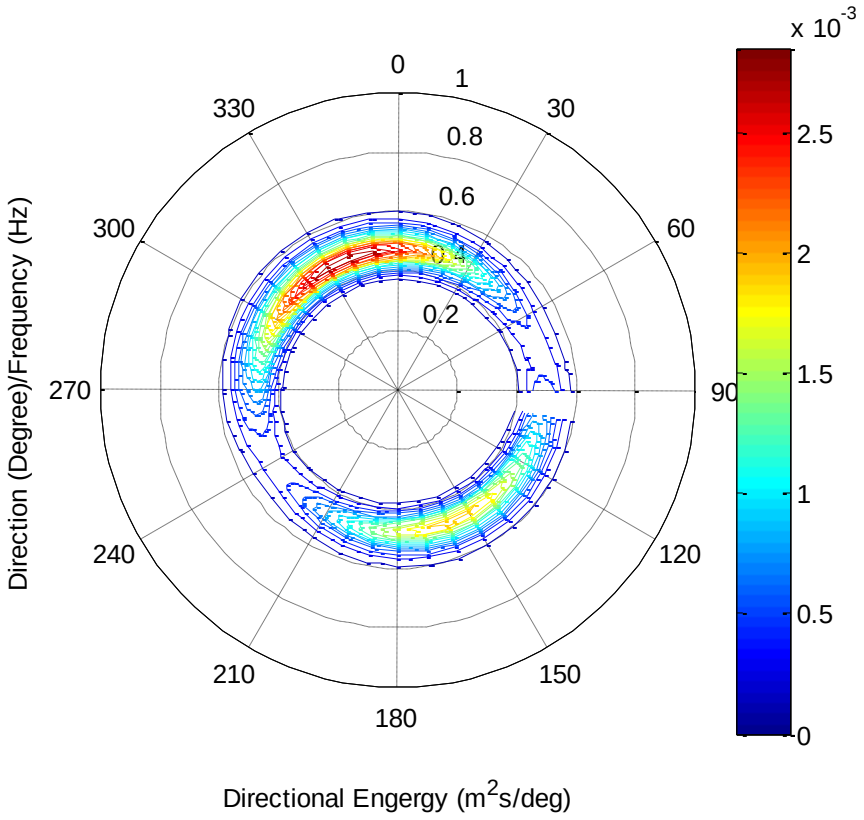

Figure 4.13 Christmas Bay Directional Wave Spectrum During Tropical Storm Bill
This figure depicts the directional wave spectrum in Christmas Bay for June 16. The peak direction of the waves was at 340° with a period of 2.13 s. The smaller mass of wave energy was from reflections of waves across the bay.

4.4 Barometric Pressure

A comparison of minimum barometric pressures for previous hurricanes along the upper Texas coastline has been compiled to assess the strength of Tropical Storm Bill Table 4.4. The fact that Tropical Storm Bill lies on the low end of table is of no surprise, as the storms being compared to Bill were devastating hurricanes. The difference between Tropical Storm Bill's and Hurricane Carla's minimum barometric pressure is 66 HPa. Lower barometric pressures in the eye of the storm create a stronger convection, thus higher winds and a larger storm.

Table 4.4 Min. Barometric Pressure of Historic Storms

Storm	Minimum Barometric Pressure (hPa)
Tropical Storm Bill	997
Hurricane Ike	935
Hurricane Carla	931
Galveston Hurricane of 1915	940
Galveston Hurricane of 1900	936

4.5 Current Velocities

Current velocities were recorded by the two Aquadopps deployed. These velocities were depth averaged and burst averaged to observe the underlying trends in flow. A one hour moving average was then applied to the signal to remove noise from the data. Directional data was computed by taking the four quadrant arctangent of the North and East components of the velocities.

To justify using depth averaged velocities, the velocity profiles were first visualized. Figures 4.12 and 4.13 depict the velocity magnitude at each bin throughout the time series for the offshore and Christmas Bay measurements, respectively. The general trend for the graph shows that velocities only increase slightly as you go up in the water column. Since there are no major reverse flows present, using the depth averaged velocity was justified. Using depth averaged velocities will create error as wind will provide a significant amount of shear. However, because measurements could not be taken near the water surface due to limitations of pulse coherent measurements, it was necessary to use depth averaged velocities. Table 4.5 quantifies some of the statistics of the velocity profiles.

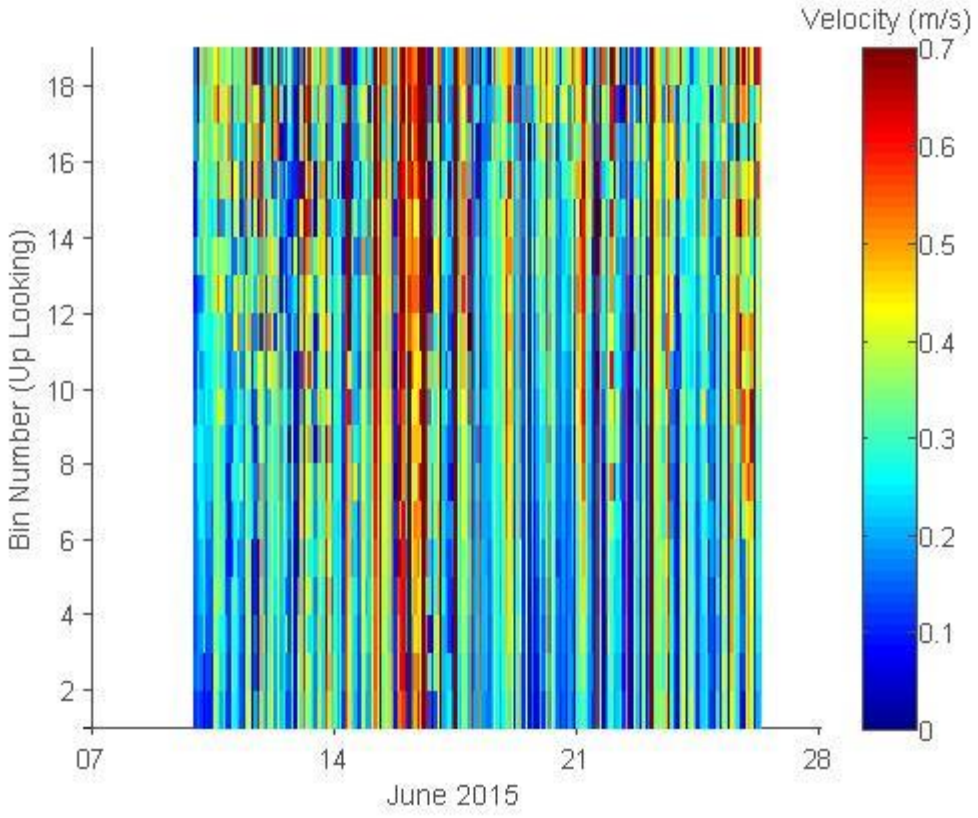

Figure 4.14 Offshore Velocity Profile
This figure depicts the velocity profile of the offshore deployment for the entire time series. Generally velocities got larger towards the surface of the water.

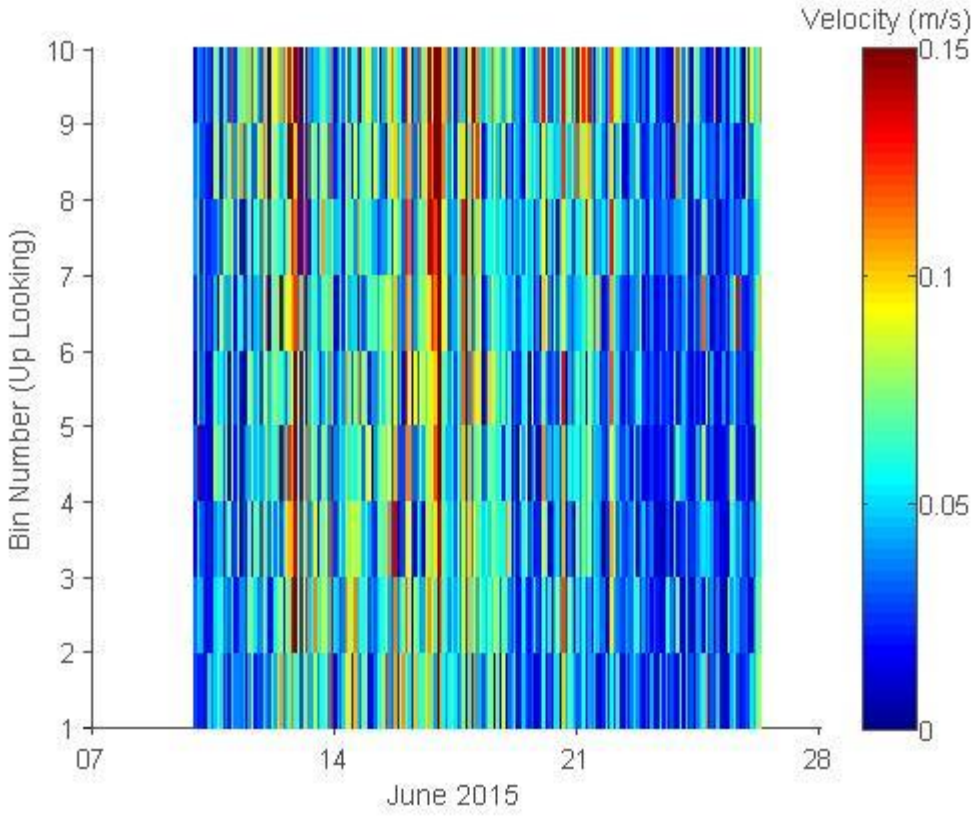

Figure 4.15 Christmas Bay Velocity Profile
This figure depicts the velocity profile of the Christmas Bay deployment for the entire time series. Generally velocities got larger towards the surface of the water.

Depth averaged current velocities (Figure 4.14) offshore had dramatic changes in magnitude and direction throughout the time series. Before the storm (June 10-14), offshore currents began flowing in a southwest direction at an average of 0.10 m/s. However, for short periods of time the current would change direction and begin to flow in the north or northeast direction. During this time current velocities peaked at 0.30 m/s on June 11, however wind, tides, and waves were all exhibiting typical conditions. It is unclear what is responsible for this brief increase in velocity.

During the storm, current velocities offshore peaked on June 15, the day before Tropical Storm Bill made landfall flowing in the northeast direction due to the storm

surge flood. The flood was assumed to begin when the angle of the current makes a sudden jump from flowing south and south east to east and north east. This occurred on June 14 at 6:40 PM. Maximum current velocity during the flood of the storm was measured at 0.29 m/s on June 15. This flow then began to taper off reaching a minimum velocity of 0.07 m/s on June 16 at 8:30 AM CDT. This point is where the surge begins to retreat. The mean of the storm current during the surge flood was 0.21 m/s. Quickly after landfall, the predominant North East current turned to an equally strong South West flow indicating the ebb of the surge. From the time the ebb started until June 18, mean current velocity was 0.18 m/s. Mean current velocity from the 15-17 was 0.19 m/s. During the surge ebb no flow reversal was evident until June 21, when the normal current fluctuations from tides became evident again.

Table 4.5 Depth Averaged Velocity Statistics

Statistic	Offshore	Christmas Bay
Average Depth Averaged Velocity (m/s)	0.16	0.06
Mean of Standard Deviation of Bins	0.09	0.02

The average flow rate after the storm (June 18-27) was again 0.10 m/s, similar to the prestorm conditions. The major spikes in velocity occurred poststorm on the 19, 20, and 21. The velocities on these days reached 0.33 m/s both on the 19 and 20, and 0.36 m/s on the 21. How these high velocities developed is unclear, though they could potentially be outliers from erroneous measurements.

Christmas Bay current velocities had a predominantly South East flow for the entirety of the time series, and the magnitude of the flow in Christmas Bay was much smaller than the offshore magnitude. Mean current velocity in Christmas Bay was 0.03 m/s. Maximum velocity in the bay was measured at 0.08 m/s on June 14. Christmas Bay exhibited a directional flow anomaly, where for short periods the flow would change to a north or northwest direction. A strong correlation between the tidal flood and this change in direction was noticed. This suggests that during flooding tides a local circulation develops within Christmas Bay. Further work of developing numerical models, as well as more instrument deployments will assist in better understanding how these various circulations in the bay develop.

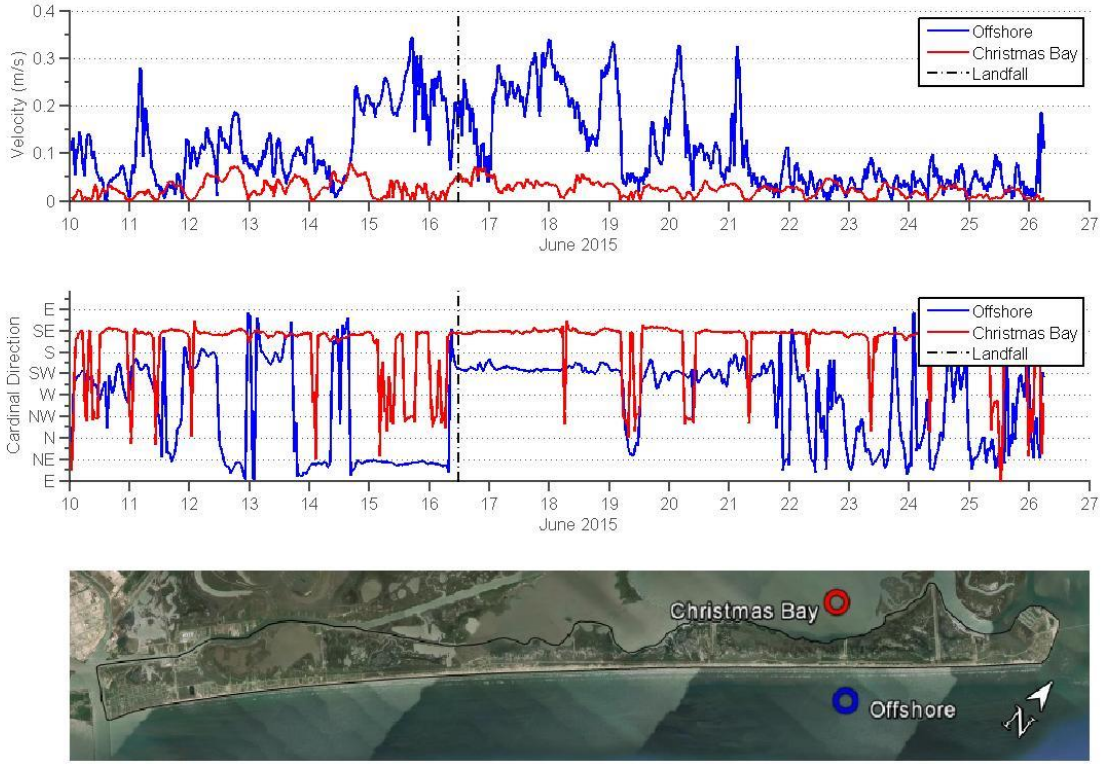

Figure 4.16 Current Magnitude and Direction

This figure depicts the velocity magnitudes and directions for the entire time series for both pods. Current velocities were an order of magnitude higher in the ocean than in the bay.

4.6 Sediment

The Malvern Mastersizer measured the mean grain size of the deployment grab samples. The offshore sediment had a mean grain size of 123.34 μm and submerged density of 2067 kg/m^3. This sediment was comprised mostly of fine sand with traces of silt. The Christmas Bay sediment had a mean grain size of 63.44 μm and a submerged density of 1843 kg/m^3. The full Malvern Mastersizer results can be seen in Appendix A.

Calibration curves were developed for both OBS using the grab samples collected at each site. Both calibrations performed extremely well, and the curves had an R^2 value of 0.9988. Many times when calibrating with coarser sediment the calibration curves will begin to taper off at larger suspended sediment concentration (SSC) since the large particles block any extra light penetrating at higher concentrations. However, with the fine sediment found in the Gulf of Mexico and Christmas Bay the curves remained linear for the entire calibration. Suspended sediment concentration was calculated using the measured OBS reading and the calibration curves developed (Figures 4.15 and 4.16).

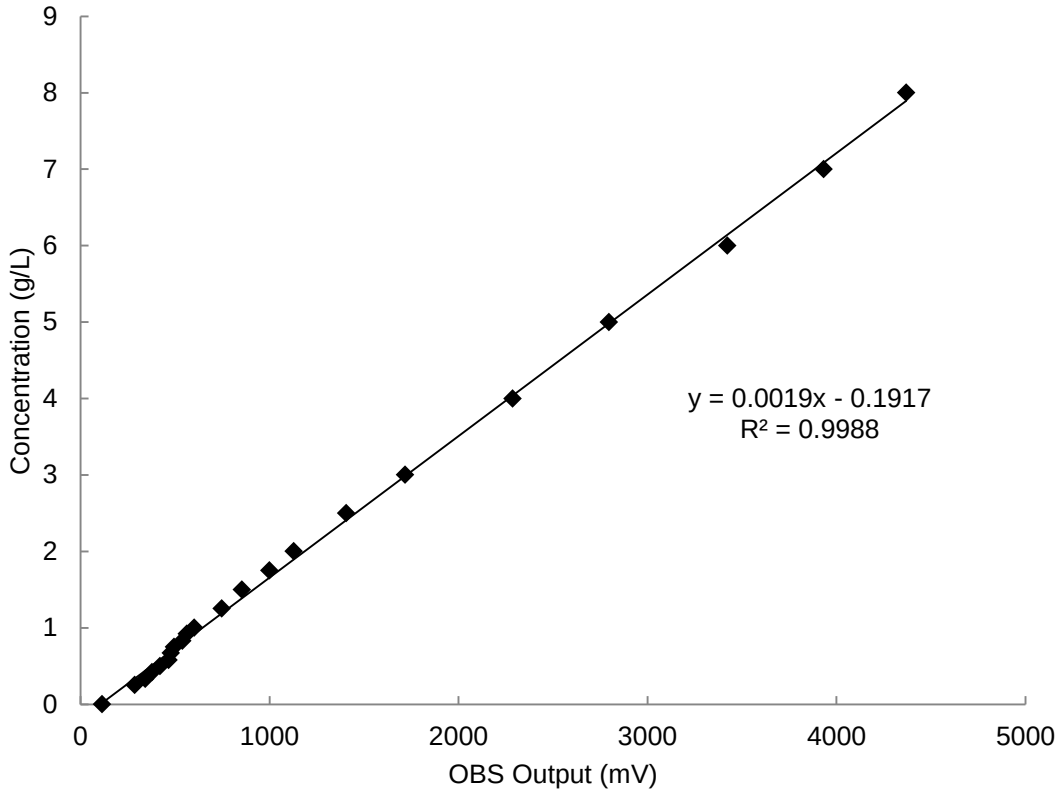

Figure 4.17 Offshore OBS Calibration Curve
This is the calibration curve created from the sediment acquired at the offshore deployment.

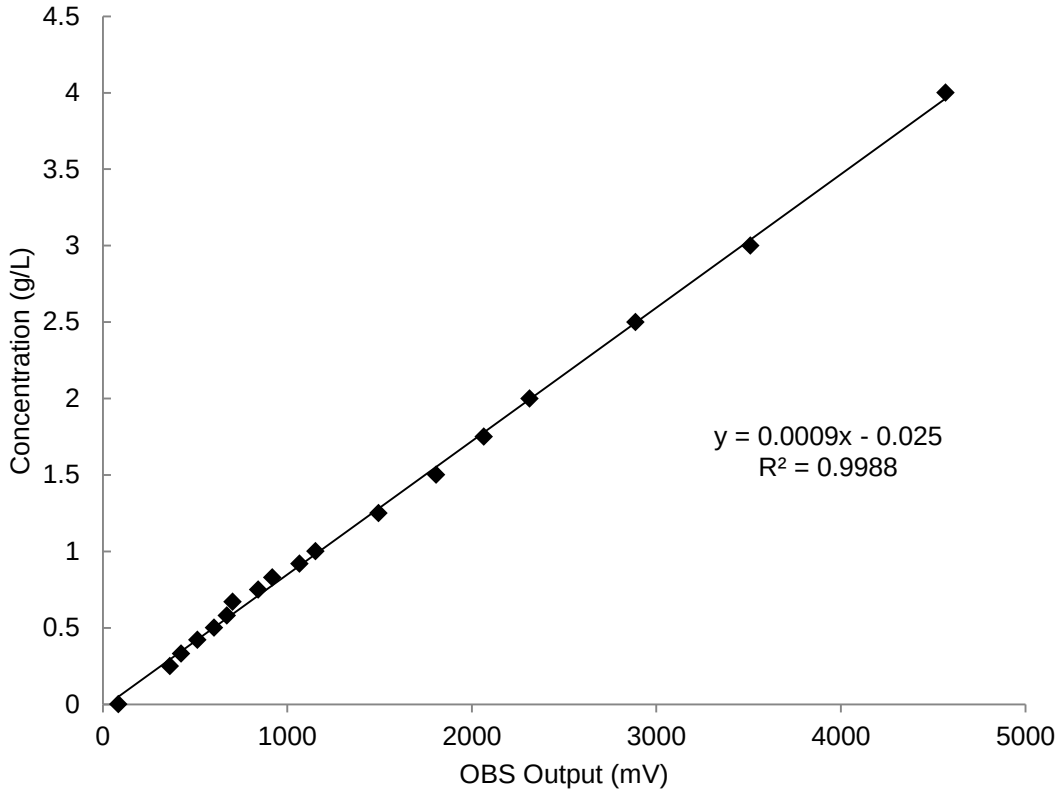

Figure 4.18 Christmas Bay OBS Calibration Curve
This is the calibration curve created from the sediment acquired at the Christmas Bay deployment.

Early in the deployments SSC (Figure 4.17) was nearly zero. Starting on June 12, the SSC at the offshore deployment started to rise. This corresponded with the initial small spike in significant wave height that occurred on the same day. The SSC continued to rise with the rising significant wave height for the next few days, with minor peaks and lows until reaching a maximum on the 17th. Maximum suspended sediment concentration for the offshore pod was measured to be 8.59 g/L which occurred on June 17 at 11:10 AM.

The Christmas Bay SSC remained under 1 g/L until the day of the 16th, just before landfall, when it quickly spiked. Maximum suspended sediment concentration for

the Christmas Bay pod was 3.09 g/L which occurred on June 17 at 3:00 AM. By Midday on the 18th the SSC in the bay seemed to have returned to typical conditions. There is an observable drift in the Christmas Bay OBS output though towards the end of the time series. A layer of caked sediment was noticed on the OBS head when the pod was recovered which could explain the higher SSC ratings after the sediment had seemed to settle.

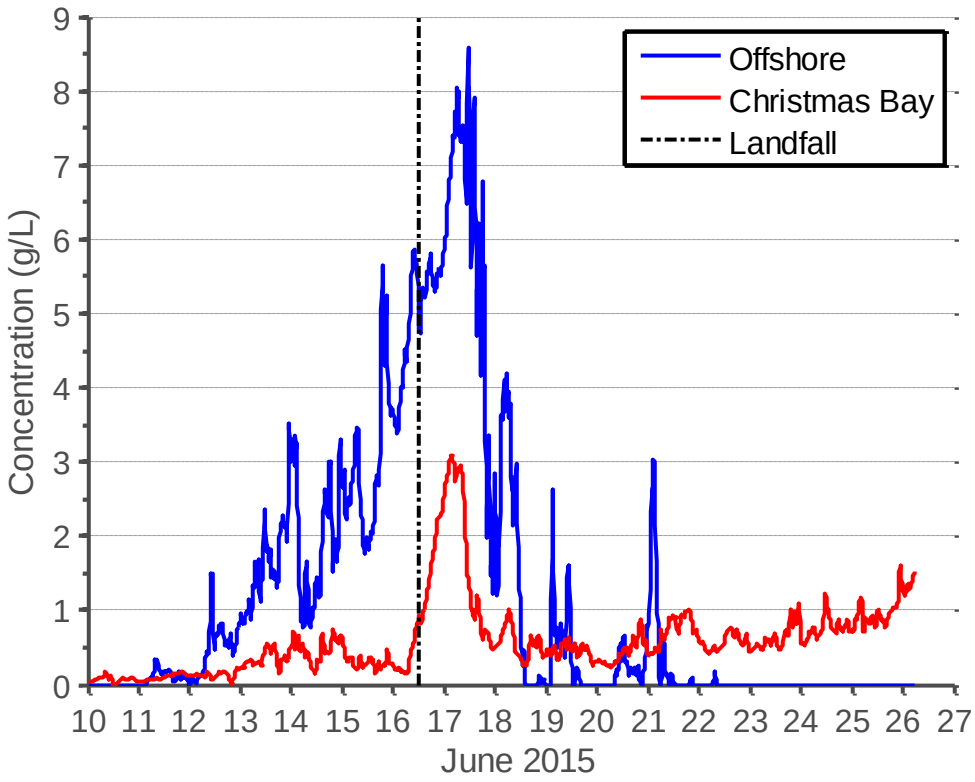

Figure 4.19 Suspended Sediment Concentration
Suspended sediment concentrations for both pods peaked after the storm had made landfall. Peak concentrations reached 8.59 g/L for the offshore deployment and 3.09 g/L for the Christmas Bay deployment.

Bed stress was calculated for the offshore and Christmas Bay time series (Figure 4.18). The offshore bed stress peaked before and after landfall of the tropical storm. After the storm, the bed stress had four spikes with an approximately 24 hour lag in between them. These spikes correlate with the four velocity spikes seen after the storm. The bed stress in Christmas Bay did not spike pre-storm, but did show a slight increase after the storm had made landfall. This correlates with a dramatic ebbing tide in the bay, as well as the start of the surge ebb creating a short burst of high flow in the bay.

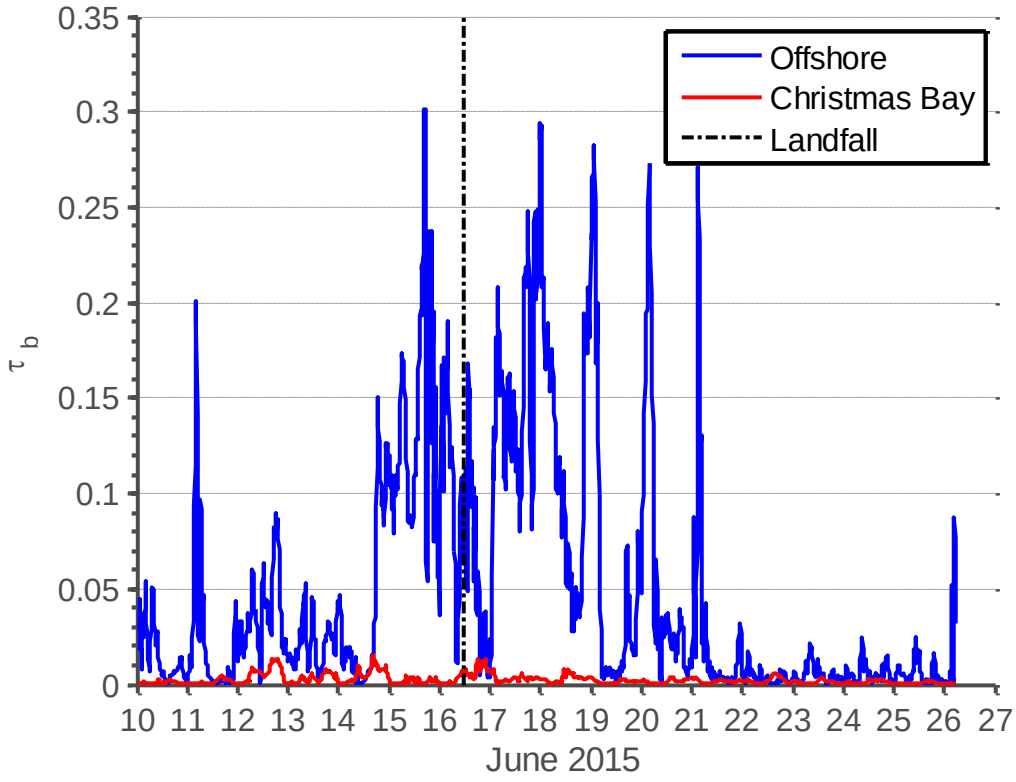

Figure 4.20 Bed Stress
Bed stress was calculated using the density of the sediment, the drag coefficient and the velocity of the water.

The Shields parameter for both locations remained well below 0.03 for the entirety of the time series (Figure 4.19). This suggests that the suspended sediment concentrations measured do not originate from the deployment locations. Therefore,

further analysis is necessary to try and quantify the sediment origin. Since the Shields parameter is a function of bed stress, the fluctuations are similar as the previous analysis.

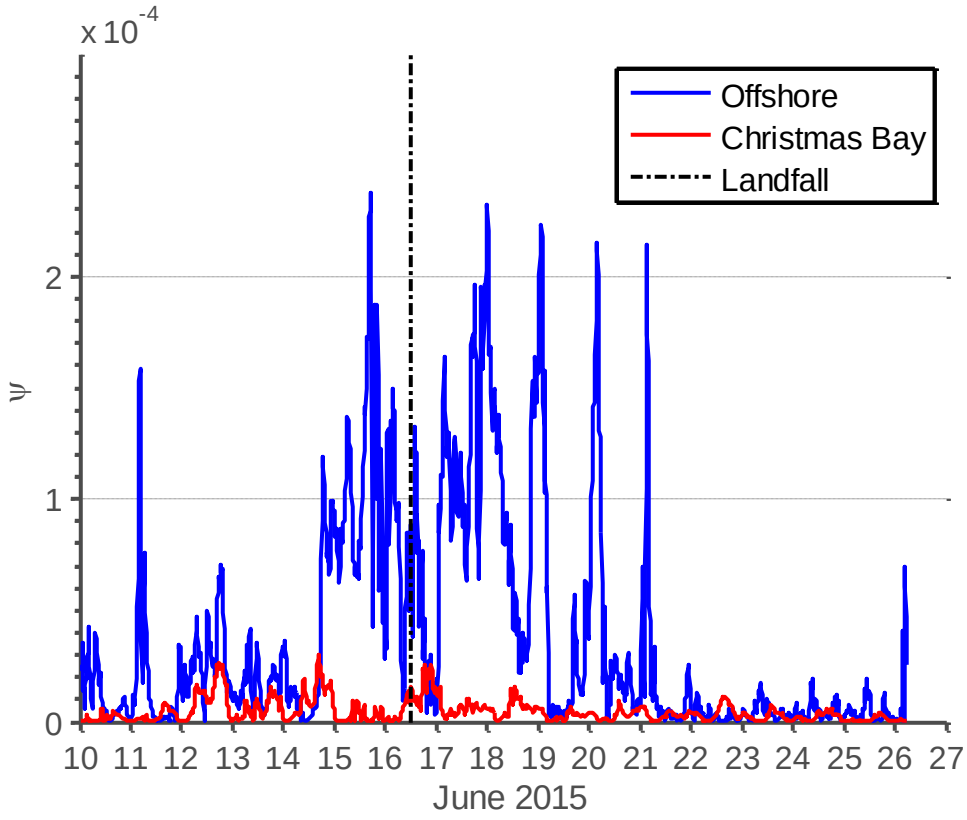

Figure 4.21 Shields Parameter
The shields parameter was calculated using the bed stress, the specific gravity of the sediment, the mean grain size, and gravity. The shields parameter for both pods was well below 0.03 for the entire time series, thus suggesting that the sediment which was measured came from a different source.

5. DISCUSSION AND CONCLUSION

5.1 Introduction

This experiment was the first to capture physical responses in Christmas Bay and the Gulf of Mexico simultaneously during a tropical storm. The hydrodynamic response demonstrates the benefits of back bay protection, while the sedimentary response indicates the storm forcing response of sediment transport. More experiments will be required to fully understand the sediment transport in this area under various forcing scenarios.

This chapter discusses the results found in the analysis from the previous chapters and concludes the report. This chapter also gives commentary on issues that arose in the deployment and data acquisition, as well as outlines possible future research projects for the monitoring of Follet's Island.

5.2 Methods

Sediment characteristics were only indicative of the samples collected at deployment. Taking grab samples at recovery as well would help develop a comparison of sediment characteristics before and after storm conditions. Another note should be made that while the OBS were calibrated using sediment grab samples at each site, measured suspended sediment concentrations most likely came from another source. This could very well lead to error in the suspended sediment concentrations as the mean grain size could differ from the grab samples. Comparisons of the two calibration curves created by the grab samples demonstrate the sensitivity of the OBS measurements. Because of this, it would be beneficial for future studies to create calibration curves using sediment from probable sources.

The sediment calibration methods used from (Pratt 1990) do not necessarily capture the actual suspended sediment concentration measure by the OBS in the field. While the sediment from Christmas bay was rather easy to keep in suspension, the larger sediment from the offshore site would drop out of suspension very quickly. It was noticed while calibrating the OBS that not all of the sediment within the chamber would

be suspended at any given time. It would be beneficial to design and construct a more sophisticated OBS calibration chamber using (Butt et al. 2002, Green and Boon 1993). Butt et al. (2002) used glycerol to help keep heavier sediment in suspensions throughout the calibration. Green and Boon (1993) created various samples of known silt and sand mixtures to better determine the measured sediment characteristics from the OBS.

5.3 Findings

This report quantified storm surge, current velocity, wave height and suspended sediment concentration response to Tropical Storm Bill in both the Gulf of Mexico and Christmas Bay. The results of this study demonstrate the dynamic interaction between ocean-barrier-bay systems. While this project measured this interaction directly and was able to shed light on this relatively unknown phenomenon, it also created many new questions to research.

Barrier island protection is vital to protecting the low lying mainland of Texas. The throttling of current velocities, wave height, and storm surge by back bay protection is evident by the dataset. If Follet's Island were to completely erode, the surrounding area's valuable infrastructure and wetland ecosystems would become even more vulnerable to storm damage. Hurricane Ike already demonstrated how breaching of Follet's Island can cause extreme damage to the inland infrastructure by removing the buffer that is the barrier. Even with a low magnitude storm such as Bill, inland storm surge, wave heights attacking the mainland, and current velocities were significantly lower in the bay than offshore. Numerical models can be used for various storm intensities to estimate the level of protection which barrier and back bay protection provide to the mainland.

Storm surge presents the greatest threat to human life and property during a storm (National Hurricane Center 2015), and storm surge mitigation is potentially the most important defense mechanism that barrier islands provide to inland communities and ecosystems. Storm surge creates extremely high current velocities atypical to the region it affects, especially during overwash and inundation events (Sallenger 2000). Follet's Island dampened the storm surge of Bill by 0.5 m when comparing the bayside

to the ocean side. This smaller surge could be from wind effects pushing the water in the bay towards the mainland, thus having lower water levels near the backside of the island, and where the measurements were taken. While this may be a small amount, this was also a small storm surge. During bigger storms this buffer could prevent damaging flood waters to the mainland; however, the full effect of surge lowering is something which can be continually monitored to gain a full understanding.

The high currents which are associated with surge create large scale erosion and expose infrastructure to wave attacks. The lower current velocities in the bay, presumably from lower surge and tidal fluctuations, prevent excess scour and erosion along the mainland. It seems inlets create a throttling effect to the incoming flood, thus decreasing water velocities. This prevents major erosion on the landward side of the island. While the currently velocities were measure to be lower in the bay, there are still questions of how these currents are being generated. As mentioned in the previous section, it seems local circulation patterns develop in the bay from flooding tides. Further monitoring of the local circulation in the bay will be necessary. Simultaneously measuring velocities from the surrounding inlets and the northern side of the bay could help indicate how this circulation is created.

Wave heights between the two locations differed by an order of magnitude, and wave energy differed by multiple orders of magnitude. The waves in the bay had a very short fetch preventing development into larger waves with more energy. This obviously prevents large wave attacks from hitting the mainland, thus halting erosion and other potential damage from larger waves. Because of the location, this deployment was not able to measure the full wave height which was hitting the mainland side of the bay. Future studies might consider measuring wave heights along the mainland side to see how waves develop across the bay during these storms.

The sedimentary response to the storm suggested that the suspended sediment measured by the OBS was not from the deployment locations. Future experiments are necessary to properly model sediment transport in these bodies of water. In future tests samples of sediment will need to be taken from areas around the deployment sites

before, after, and during the deployment. In the offshore deployment, data suggests that the majority of the suspended sediment concentration was carried by the ebb of the storm in the southwest direction. In the bay, the major direction of sediment transport was to the southeast, and this is the one of the most perplexing findings of this experiment. This could suggest that the suspended sediment in the bay could have come from the western side of the bay or from Cold Pass and driven by a local circulation in the bay. While the origin and ultimate destination of the suspended sediment is unknown, sediment transport can be estimated. The suspended sediment concentration was plotted against the depth averaged velocity in an attempt to visualize the direction of sediment transport (Figure 5.1).

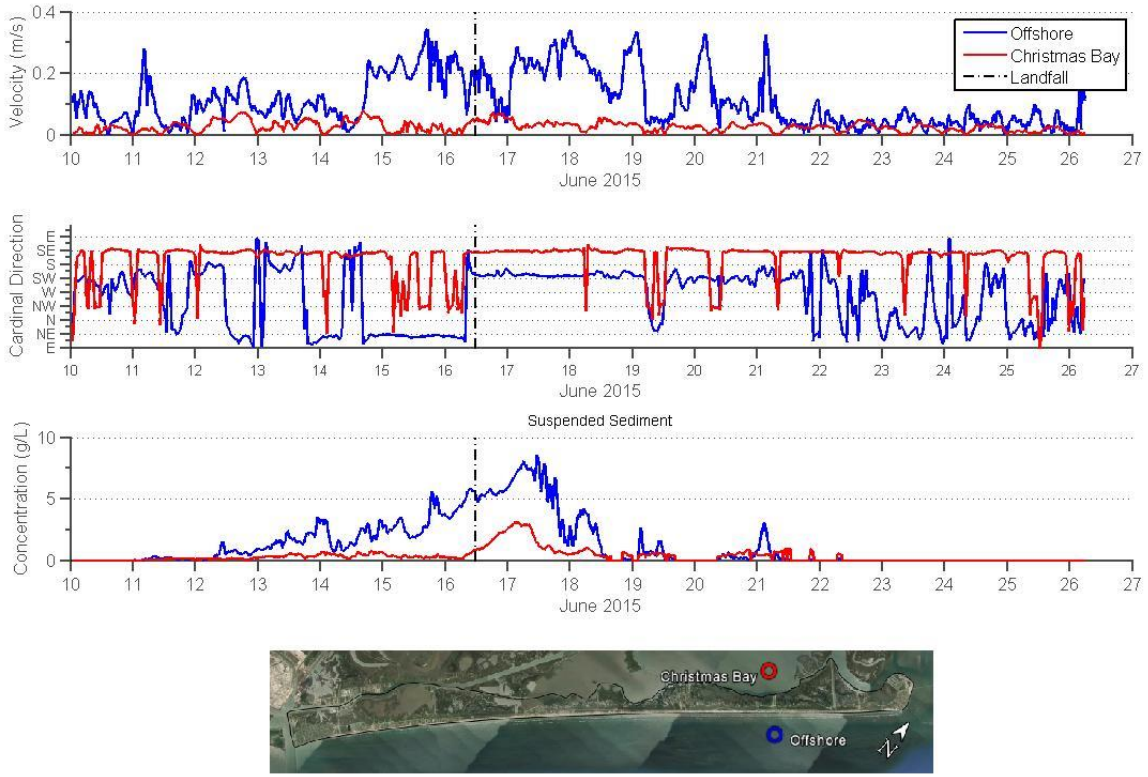

Figure 5.1 Suspended Sediment Transport
The suspeded sediment concentration was plotted with the current magnitudes and direction to better observe the sediment transport from the deployments.

In the Gulf, current velocities before landfall, while the SSC was ramping up with the flood of the storm surge, were driving the sediment in the northeast direction. However, during the ebb of the storm and the highest SSC spike, sediment was being transported in the southwest direction. In Christmas Bay there was very little SSC before the storm. However, after landfall, during the ebb of the surge currents were flowing in the southeast direction for the duration of the SSC spike.

In an attempt to quantify the amount and direction sediment transported by the storm at the two points the mass flux was calculated. Methods from Jaffe et al. (1984) were used for this analysis. In the Jaffe et al. (1984) study, cross shore and longshore sediment flux was calculated using an array of optical backscatter sensors, current meters, and one pressure sensor to estimate the SSC throughout the water column. The SSC was linearly fitted to the measurements from the OBS at various depths. Cross shore and longshore sediment transport were separated using the components of the current velocity and the relative angle of the coastline.

For the analysis in this study a few assumptions are needed to be made, because only one current meter and OBS was used at each location. The first assumption was using a constant SSC for over the distance measured by the OBS. The Campbell Scientific OBS3+ is stated to be able to 'look' as far as 50 cm in very clear water using light sent out at 165° rectangular pyramid from the head of the device Figure 5.2. Turbid water, however, will decrease the distance that the OBS can measure. Because of this, the second assumption was a distance of 10 cm was used for the flux calculation. The final assumption was to use the depth averaged velocity calculated earlier for the transport.

Figure 5.2 Campbell Scientific OBS3+ Measuring Scheme
This figure depicts the measuring scheme for the OBS used in this experiment. The rectangular prism is the area in which light is sent out, and the circular pyramid is the area in which the reflected light is observed and measured.

To separate the cross and longshore transport the relative angle of the coastline was used. The coastline of Follet's island was approximated to lie at a heading of 51° clockwise from North. This angle was used for both the ocean and bay coast since at the locations, they are very similar. To compute the cross shore and longshore transport the following equation was used:

$$Time\ Averaged\ Flux\ = \frac{1}{T}\int_{t=0}^{T}\int_{z=0}^{Z} SSC * v\ dtdz \tag{32}$$

where, the $Time\ Averaged\ Flux$ is a mass flux given in kg/m/s, the SSC is the measured suspended sediment concentration, v is the depth averaged velocity component in the cross or longshore direction, T is the time of one burst (600 s), and Z is the OBS measuring distance (0.10 m).

The time averaged longshore sediment flux suggested an offshore net littoral drift to the Southwest, but very little cross shore transport in the bay. Figure 5.3 displays the time averaged longshore sediment flux where, negative is to the northeast and positive is to the southwest relative to the orientation of the island. The dashed lines on this figure and figure 5.4 represent error bars based on the standard deviation of the time series. During the storm surge flood there is a net flux to the east, however, following the trend of the currents, this quickly changes to a larger net flux towards the west following the ebb of the surge. A total of 11.11 kg/m was transported to the southwest at the offshore pod, and 0.08 kg/m was transported to the northeast at the Christmas Bay pod.

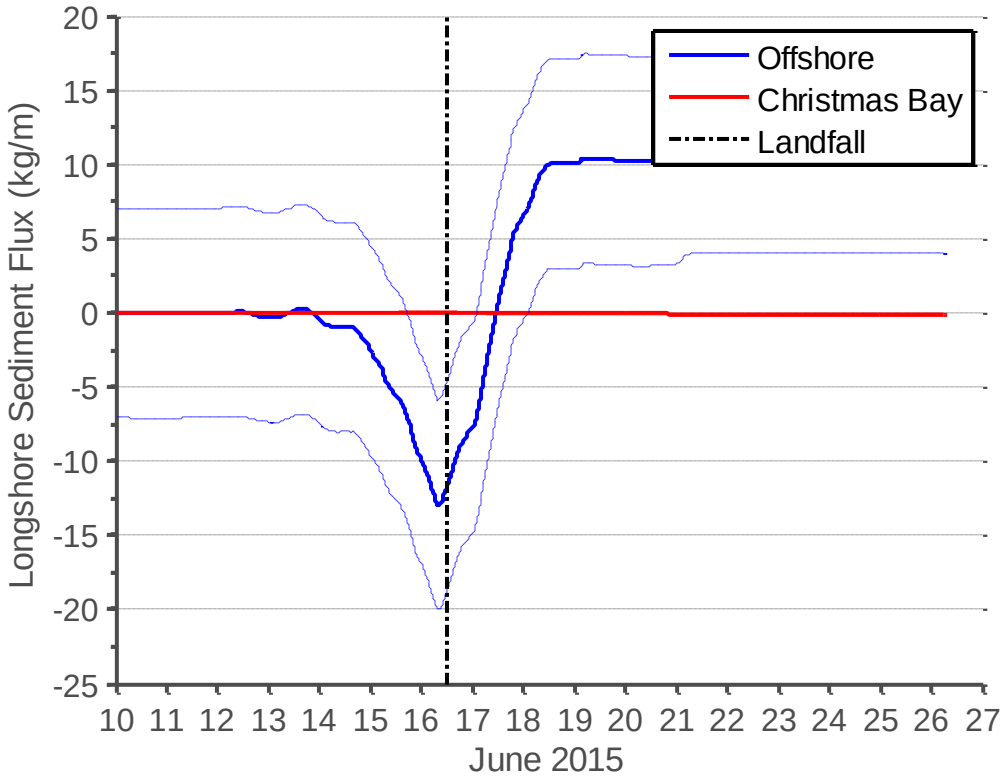

Figure 5.3 Longshore Time Averaged Sediment Flux
This figure depicts the integrated time averaged longshore sediment flux. Negative numbers refer to the Northeast direction and positive numbers refer to Southwest, based on the islands geometry. While Christmas Bay exhibited very little longshore flux, the offshore pod measured 11.11kg/m flux towards the Southwest. The dashed lines represent error bars based on the standard deviation of the each line. The standard deviation for Christmas Bay is so low that the line is not visible.

The time averaged cross shore sediment transport (Figure 5.4) suggested that sediment was transported towards the ocean at both points. The offshore pod measured 8.84 kg/m of sediment being transported towards the Gulf of Mexico, and the Christmas Bay pod measured 0.55 kg/m of sediment being transported towards the back side of the island.

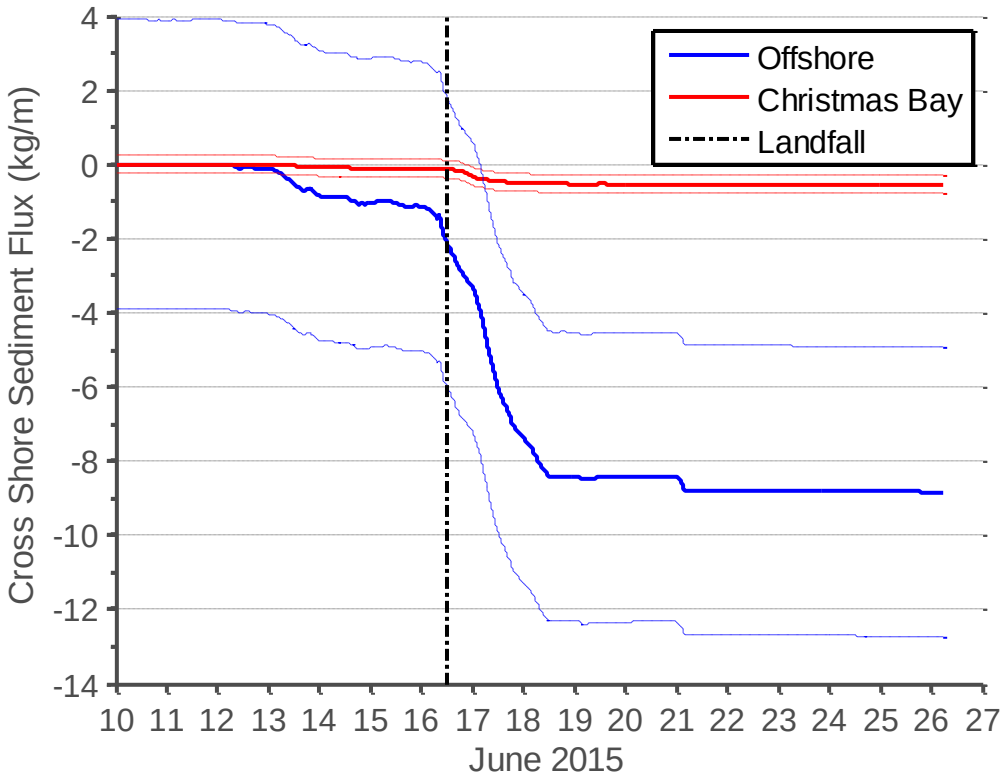

Figure 5.4 Time Averaged Cross Shore Sediment Flux
This figure depicts the integrated time averaged longshore sediment flux. Negative numbers refer to the offshore direction and positive numbers refer to the direction of mainland Texas, based on the islands geometry. Both pods measured a flux towards the offshore. The Christmas Bay pod measured 0.55 kg/m, and the offshore pod measured 8.84 kg/m towards the Gulf of Mexico. The dashed lines represent error bars based on the standard deviation of each line.

5.4 Conclusion

This deployment directly measured the hydrodynamics and sediment transport of Tropical Storm Bill, but only in two locations. This dataset sheds light on how oceans and bay separated by barrier islands respond to each other. The hydrodynamic and sedimentary responses to the Tropical Storm each have strong implications towards barrier island coastal management.

The findings of this report strongly support the need for barrier islands and back bay protection against storms. Wave heights differed by an order of magnitude, storm surge was buffered by a half a meter, and current velocities were significantly lower. All of this accounts for lower erosion and sediment transport behind the island, and thus grants vital protection to the surrounding ecology, mainland, and infrastructure. Therefore, further studies coupled with continuous monitoring are vital to developing coastal management plans which will maintain this protection. Also, development of numerical models will help create a better understanding of the ocean and bay dynamics.

The sedimentary response to the storm displayed sediment from both pods being transported towards the ocean side of the island. Without multiple sensors deployed to observe a gradient in the suspended sediment concentration, it is not possible to make any assumptions to the deposition of the sediment. Further deployments with more sensors deployed can help shape a better understanding of where sediment is coming from and being transported to.

Ultimately, more studies are needed to fully understand the ocean and back bay dynamics. With a larger array of measurements capturing more natural events, such as cold fronts and other tropical storms, the complex interaction between these two bodies of water as well as the short and long term evolution of Follet's Island can be better understood.

REFERENCES

Anderson, J. (2007). Formation and Future of the Upper Texas Coast: A Geologist Answers Questions about Sand, Storms, and Living by the Sea. College Station, TX: Texas A&M University Press.

Beven, Jack (June 17, 2015). Tropical Storm Bill Advisory Number 5. National Hurricane Center. Miami, Florida: National Oceanic and Atmospheric Administration. Retrieved June 17, 2015

Blake, E. S. and Franklin, J. L. (June 12, 2015). Tropical Weather Outlook 200 PM EDT Fri. Jun. 12 2015. National Hurricane Center. Miami, Florida: National Oceanic and Atmospheric Administration. Retrieved August 8, 2015.

Brennan, Michael (June 14, 2015). Tropical Weather Outlook 800 PM EDT Sun. Jun 14 2015. National Hurricane Center. Miami, Florida: National Oceanic and Atmospheric Administration. Retrieved June 16, 2015.

Butt, T., Miles, J., Ganderton, P., & Russell, P. (2002). A simple method for calibrating optical backscatter sensors in high concentrations of non-cohesive sediments. Marine Geology, 192(4), 419–424.

Cangialosi, John P.; Blake, Eric S. (June 13, 2015). Tropical Weather Outlook 200 PM EDT Sat. Jun 13 2015. National Hurricane Center. Miami, Florida: National Oceanic and Atmospheric Administration. Retrieved August 8, 2015.

Conference on Ocean Wave Spectra, United States, Naval Oceanographic Office, National Research Council (U.S.), & Division of Earth Sciences (Eds.). (1963). Ocean wave spectra; proceedings of a conference. [Englewood Cliffs, N.J.]: [Prentice-Hall].

Dean, R. G. and Dalrymple, R. A. (2002). Coastal Processes with Engineering Applications. Cambridge, United Kingdom: Cambridge University Press.

Fritz, H. M., Blount, C., Sokoloski, R., Singleton, J., Fuggle, A., McAdoo, B. G., … Tate, B. (2007). Hurricane Katrina storm surge distribution and field observations on the Mississippi Barrier Islands. Estuarine, Coastal and Shelf Science, 74(1–2), 12–20.

Goda, Y. (n.d.). On the Methodology of Selecting Design Wave Height (pp. 899–913). Presented at the Coastal Engineering (1988), ASCE.

Green, M. O., & Boon, J. D. (1993). The measurement of constituent concentrations in nonhomogeneous sediment suspensions using optical backscatter sensors. Marine Geology, 110(1), 73–81.

Haan, C. T. (1977). Statistical methods in hydrology. The Iowa State University Press.

Hayes, M. O. (1967). Hurricanes as Geological Agents, South Texas Coast: GEOLOGICAL NOTES. AAPG Bulletin, 51(6), 937–942.

HDR. (2014). Beach and Shoreline Changes Along the Upper Texas Coast: Recovery from Hurricane Ike (Project Number 166742). Austin: Texas General Land Office.

Hoyt, J. H. (1967). Barrier Island Formation. Geological Society of America Bulletin, 78(9), 1125–1136.

Interagency Advisory Committee on Water Data, 1982, Guidelines for determining flood-flow frequency: Bulletin 17B of the Hydrology Subcommittee, Office of Water Data Coordination, U.S. Geological Survey, Reston,Va., 183 p.

Jaffe, B. E., Sternberg, R. W., & Sallenger, A. H. (1984). The Role of Suspended Sediment in Shore-Normal Beach Profile Changes. Coastal Engineering Proceedings, 1(19).

Keim, B. D., Muller, R. A., & Stone, G. W. (2007). Spatiotemporal Patterns and Return Periods of Tropical Storm and Hurricane Strikes from Texas to Maine. Journal of Climate, *20*(14), 3498–3509.

Kennedy, A. B., Gravois, U., Zachry, B. C., Westerink, J. J., Hope, M. E., Dietrich, J. C., … Dean, R. G. (2011). Origin of the Hurricane Ike forerunner surge. Geophysical Research Letters, 38(8), L08608.

List, J. H., & Hansen, M. E. (1992). The value of barrier islands; 1, Mitigation of locally-generated wind-wave attack on the mainland (USGS Numbered Series No. 92-722). U.S. Geological Survey.

Lohrmann, A., Hacket, B., & Røed, L. P. (1990) High resolution measurements of turbulence, velocity and stress using a pulse-to-pulse coherent sonar. Journal of Atmospheric and Oceanic Technology, 7, 595-603.

Mizuguchi, M. (n.d.). Individual Wave Analysis of Irregular Wave Deformation in the Nearshore Zone (pp. 485–504). Presented at the Coastal Engineering (1982), ASCE.

Morton, R. A. (1994). Texas Barriers. In P. D. R. A. D. Jr (Ed.), Geology of Holocene Barrier Island Systems (pp. 75–114). Springer Berlin Heidelberg.

Morton, R. A., Gibeaut, J. C., & Paine, J. G. (1995). Meso-scale transfer of sand during and after storms: implications for prediction of shoreline movement. Marine Geology, 126(1–4), 161–179.

Morton, R. A., & Pieper, M. J. (1975). Shoreline changes in the vicinity of the Brazos River delta (San Luis pass to Brown Cedar Cut). An analysis of historical changes of the Texas Gulf shoreline.

National Hurricane Center. (2015). Storm Surge Overview. NOAA. Retrieved from: http://www.nhc.noaa.gov/surge/

Needham, H. F., & Keim, B. D. (2012). A storm surge database for the US Gulf Coast. International Journal of Climatology, *32*(14), 2108–2123.

Oregon State Univeristy (2005). Streamflow Evaluations for Watershed Restoration Planning and Design. Retrieved from http://streamflow.engr.oregonstate.edu/index.htm

Paine, J. G. (1993). Subsidence of the Texas coast: inferences from historical and late Pleistocene sea levels. Tectonophysics, 222(3–4), 445–458.

Paine, J. G. (2012). Historical Shoreline Change through 2007, Texas Gulf Coast: Rates, Contributing Causes, and Holocene Context. Gulf Coast Association of Geological Societies, 1, 13-26.

Palutikof, J. P., Brabson, B. B., Lister, D. H., & Adcock, S. T. (1999). A review of methods to calculate extreme wind speeds. Meteorological Applications, 6(2), 119–132.

Pratt, T. C. (1990). Near-Bed Optical Backscatter Sensor and Vector-Measuring Velocity Meter Calibration. Technical Report HL-90-10. U.S. Army Corps of Engineers.

Roberts, H. H., Huh, O. K., Hsu, S. A., Rouse, L. J., & Rickman, D. (1987). Impact of Cold-Front Passages on Geomorphic Evolution and Sediment Dynamics of the Complex Louisiana Coast (pp. 1950–1963). Presented at the Coastal Sediments (1987), ASCE.

Rodriguez, A., Fassell, M., & Anderson, J. (2001). Variations in shoreface progradation and ravinement along the Texas coast, Gulf of Mexico. Sedimentology, 48(4), 837–853.

Rodriguez, A., Anderson, J., Siringan, F., & Taviani, M. (2004). Holocene Evolution of the East Texas Coast and Inner Continental Shelf: Along-Strike Variability in Coastal Retreat Rates. Journal of Sedimentary Research, 74(3), 405–421.

Rusello, P., Lohrmann, A., Siegel, E., Maddux, T. (n.d.). Improvements in acoustic Doppler velocimetry. Proceedings of the Sevent International Conference on Hydroscience and Engineering, Philadelphia, PA, September 2006. Philadelphia: Drexel University, 2006.

Sallenger, A. H., Jr. (2000). Storm Impact Scale for Barrier Islands. Journal of Coastal Research, 16(3), 890–895.

Sheremet, A., Mehta, A., Liu, B., & Stone, G. (2005). Wave–sediment interaction on a muddy inner shelf during Hurricane Claudette. Estuarine, Coastal and Shelf Science, 63(1–2), 225–233.

Texas General Land Office. (2015). Coastal Erosion. Retrieved from: http://www.glo.texas.gov/what-we-do/caring-for-the-coast/coastal-erosion/

U.S. Army Corps of Engineers. (1983). Galveston County shore erosion study-feasibility report and environmental impact statement. Gulf Shoreline Study Site Rep. 2. Galveston District Corps of Eng.

U.S. Department of Energy. (2008). Strategic Petroleum Reserve Annual Report for Calendar Year 2008.

Valle-Levinson, A., Wong, K.-C., & Bosley, K. T. (2002). Response of the lower Chesapeake Bay to forcing from Hurricane Floyd. Continental Shelf Research, 22(11–13), 1715–1729.

Walker, N. D. (2001). Tropical Storm and Hurricane wind effects on water level, salinity, and sediment transport in the river-influenced Atchafalaya-Vermilion Bay System, Louisiana, USA. Estuaries, 24(4), 498–508.

Wallace, D. J., Anderson, J. B., & Fernández, R. A. (2010). Transgressive Ravinement versus Depth of Closure: A Geological Perspective from the Upper Texas Coast. Journal of Coastal Research, 1057–1067.

Watson, R.L. (2003). Severe Beach Erosion at Surfside, Texas Caused by Engineering Modifications to the Coast and Rivers. Geological Society of America Annual Conference. Geological Society of America Abstracts with Programs, Vol. 39, No. 6, p. 96

Welch, P. D. (1967). The use of fast Fourier transform for the estimation of power spectra: A method based on time averaging over short, modified periodograms. IEEE Transactions on Audio and Electroacoustics, 15(2), 70–73.

Wiltgen, N., et al. (2015). Tropical Depression Bill Inland Over Texas; Major Flood Threat for Texas, Oklahoma, Ozarks. Retrieved from http://www.weather.com/storms/hurricane/news/tropical-storm-bill-flooding-heavy-rain-threat

Wright, L. D., Swaye, F. J., & Coleman, J. M. (1970). Effects of Hurricane Camille on the Landscape of the Breton-Chandeleur Island Chain and the Eastern Portion of the Lower Mississippi Delta. Coastal Studies Institute. Technical Report 76. Baton Rouge, LA.

APPENDIX A: MALVERN MASTERSIZER RESULTS

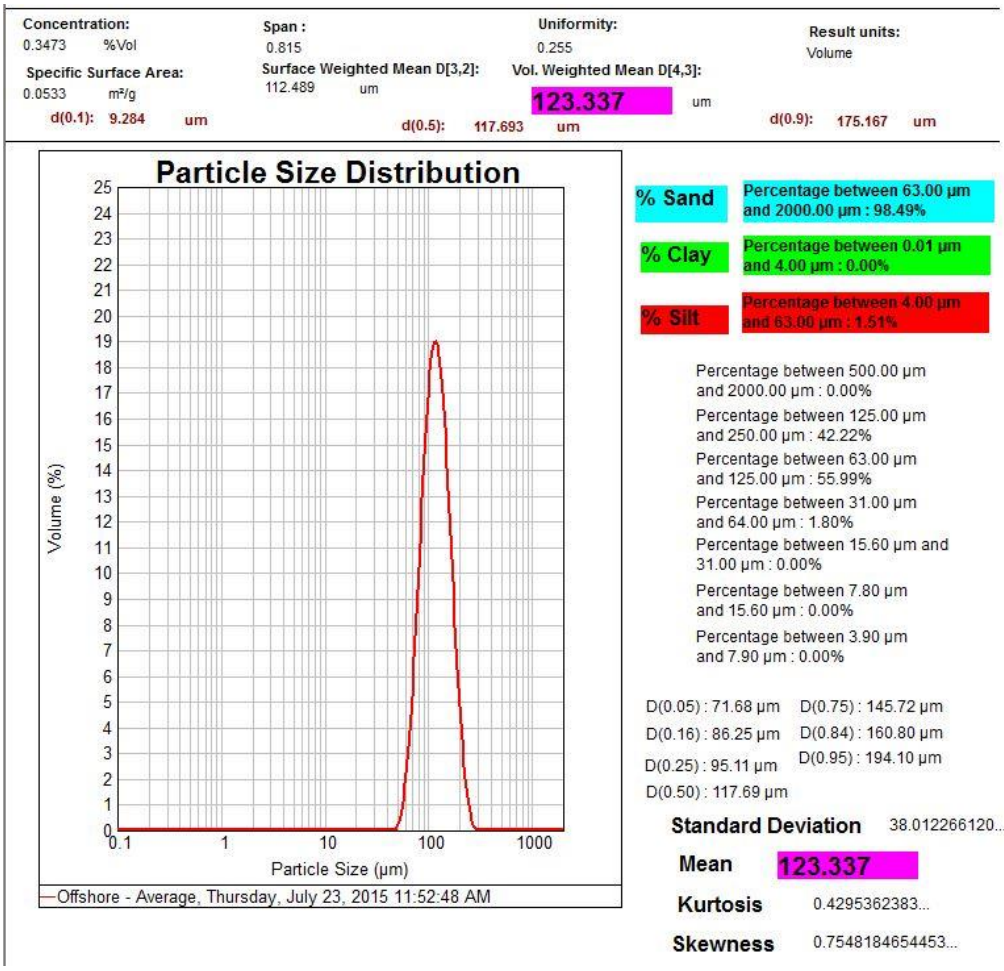

Figure A.1 Offshore Sediment Size Distribution

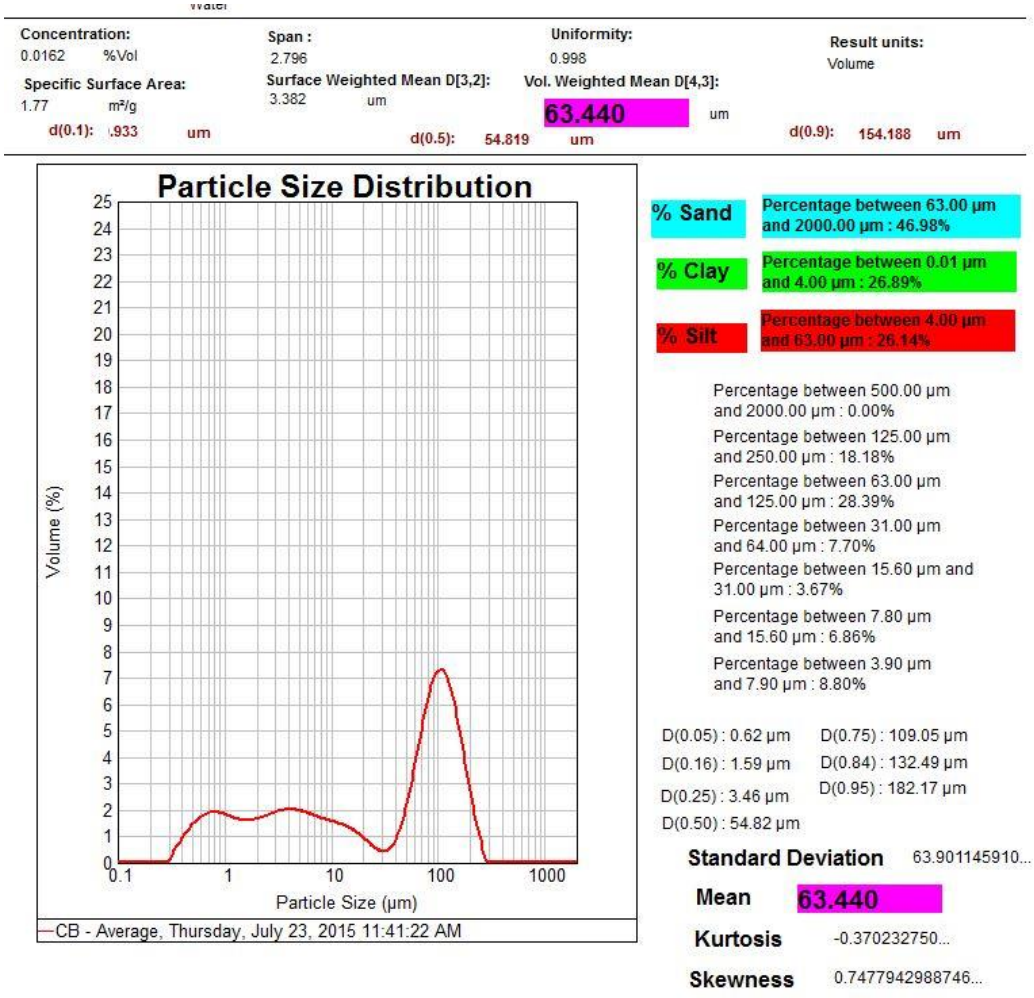

Figure A.2 Christmas Bay Sediment Size Distribution

APPENDIX B: DEPLOYMENT SCHEME

Deployment : Follet's
Current time : 6/8/2015 10:42:31 AM
Start at : 6/10/2015
Comment:
Offshore 1 MHz

Measurement interval (s) : 600
Cell size (mm) : 30
Orientation : UPLOOKING SHALLOW WATER
Distance to surface (m) : 4.00
Pulse distance (m) : 2.00
Profile range (m) : 1.56
Horiz. vel. range (m/s) : 0.91
Vert. vel. range (m/s) : 0.39
Number of cells : 52
Average interval (s) : 1
Blanking distance (m) : 0.400
Measurement load (%) : 45
Samples per burst : 512
Sampling rate (Hz) : 1
Compass upd. rate (s) : 1
Coordinate System : ENU
Speed of sound (m/s) : MEASURED
Salinity (ppt) : 35
Analog input 1 : PROFILE
Analog input 2 : NONE
Analog input power out : DISABLED
File wrapping : OFF
TellTale : OFF
Acoustic modem : OFF
Serial output : OFF
Baud rate : 115200

Assumed duration (days) : 17.0
Battery utilization (%) : 96.0
Battery level (V) : 13.5

Deployment : Follet's
Current time : 6/8/2015 10:42:31 AM
Start at : 6/10/2015
Comment:
Christmas Bay 2 MHz

Measurement interval (s) : 600
Cell size (mm) : 30
Orientation : UPLOOKING SHALLOW WATER
Distance to surface (m) : 1.00
Pulse distance (m) : 0.50
Profile range (m) : 0.36
Horiz. vel. range (m/s) : 1.83
Vert. vel. range (m/s) : 0.77
Number of cells : 12
Average interval (s) : 1
Blanking distance (m) : 0.100
Measurement load (%) : 49
Samples per burst : 512
Sampling rate (Hz) : 1
Compass upd. rate (s) : 1
Coordinate System : ENU
Speed of sound (m/s) : MEASURED
Salinity (ppt) : 35
Analog input 1 : PROFILE
Analog input 2 : NONE
Analog input power out : DISABLED
File wrapping : OFF
TellTale : OFF
Acoustic modem : OFF
Serial output : OFF
Baud rate : 115200

Assumed duration (days) : 25.0
Battery utilization (%) : 147.0
Battery level (V) : 13.9
Recorder size (MB) : 3773
Recorder free space (MB) : 3772.972
Memory required (MB) : 351.6

Instrument ID : AQD12670
Head ID : ASP 7398
Firmware version : 3.19 HR
ProLog ID : 1134
ProLog firmware version : 4.22

APPENDIX C: DEPLOYMENT MANUAL

Day #	Tasks	Date	Kevin	Josh	Hunter
0	Organize all instruments and mounts	TBD	x		
0	Fuel and mobilize boat	TBD	x		
0	Reserve divers		x		
0	Test Aquadopp and OBS3+ mounts		x		
0	Calibrate compasses		x		
0	Calibrate clocks		x		
0	Set recording settings		x		
1	Deploy Aquadopp 1 with OBS3+ to station 1		x	x	x
	Deploy Aquadopp 2 with OBS3+ to station 2		x	x	x
30	Recover Aquadopp 1		x	x	x
	Recover Aquadopp 2		x	x	x

Table C.1 Task Schedule

Deployment Schedule

1. Kevin will pick up Josh at his residence at 0600
2. Kevin and Josh will drive to campus and load equipment in truck
3. Divers will arrive on campus at 0630
4. Team will drive to Tim Dellapenna's house to pick up kayaks used for Christmas bay deployment (this task may be done after the offshore deployment depending on truck space)
5. Team will continue to Freeport where Parker 25 is located
6. Team will depart in Parker 25 to offshore deployment site
7. Mount will be assembled on route to offshore deployment site
8. Once at site divers will guide the instrumentation pod to seabed **(COORDINATES ARE TO BE MARKED AT DEPLOYMENT)**
9. Divers are to attempt to orient aquadopp head to point towards North
10. Divers will take sediment samples at sea bed

11. Kevin and Josh will take depth measurements along deployment transect
12. Once pod is deployed divers will gather back in the boat to cruise back towards Freeport docks
13. Once in Freeport, divers are released from duty
14. Kevin and Josh will then take the kayaks and second pod to the boat ramp on COUNTY ROAD 257S
15. Kevin and Josh will row kayaks with deployment pod to Christmas Bay deployment site
16. Pod will be deployed at site
17. Kevin and Josh will take sediment samples at deployment site
18. Kevin and Josh will take depth measurements along route back to the boat ramp
19. Kevin and Josh will row back to the boat ramp to load kayaks back into car and drive back to Galveston dropping the kayaks at Tim Dellapenna's house along the way

Tidal Conditions for April-June 2015

StationId:8771972
Source:NOAA/NOS/CO-OPS
Station Type:Harmonic
Time Zone:LST/LDT
Datum:mean lower low water (MLLW) which is the chart datum of soundings

NOAA Tide Predictions

SAN LUIS PASS (TCOON),Texas,2015

Times and Heights of High and Low Waters

April

	Time	Height (ft)	Height (cm)
1 W	02:54 AM	1.1	34
	10:00 AM	0.6	18
	04:18 PM	1.0	30
	10:23 PM	0.7	21
2 Th	03:50 AM	1.1	34
	10:47 AM	0.6	18
	04:20 PM	1.0	30
	10:52 PM	0.6	18
3 F	04:43 AM	1.2	37
	11:29 AM	0.7	21
	04:36 PM	1.1	34
	11:19 PM	0.5	15
4 Sa ○	05:28 AM	1.2	37
	12:06 PM	0.8	24
	04:55 PM	1.1	34
	11:42 PM	0.5	15
5 Su	06:10 AM	1.2	37
	12:42 PM	0.9	27
	05:08 PM	1.1	34
6 M	12:05 AM	0.4	12
	06:57 AM	1.3	40
	01:28 PM	1.0	30
	05:08 PM	1.1	34
7 Tu	12:33 AM	0.3	9
	07:59 AM	1.3	40
	02:48 PM	1.1	34
	05:10 PM	1.1	34
8 W	01:07 AM	0.3	9
	09:20 AM	1.3	40
9 Th	01:51 AM	0.3	9
	10:36 AM	1.3	40
10 F	02:43 AM	0.3	9
	12:21 PM	1.4	43
11 Sa	03:40 AM	0.3	9
	01:25 PM	1.4	43
12 Su ◑	04:44 AM	0.3	9
	01:56 PM	1.3	40
13 M	06:19 AM	0.4	12
	02:08 PM	1.3	40
	08:25 PM	1.0	30
	11:25 PM	1.1	34
14 Tu	07:37 AM	0.4	12
	02:19 PM	1.3	40
	08:40 PM	0.9	27
15 W	01:32 AM	1.2	37
	08:37 AM	0.5	15
	02:39 PM	1.2	37
	09:04 PM	0.7	21
16 Th	02:49 AM	1.3	40
	09:42 AM	0.6	18
	03:06 PM	1.2	37
	09:37 PM	0.6	18
17 F	04:05 AM	1.4	43
	10:50 AM	0.8	24
	03:36 PM	1.2	37
	10:21 PM	0.4	12
18 Sa ●	05:15 AM	1.5	46
	11:49 AM	0.9	27
	04:07 PM	1.2	37
	11:07 PM	0.2	6
19 Su	06:15 AM	1.5	46
	12:43 PM	1.0	30
	04:37 PM	1.2	37
	11:50 PM	0.1	3
20 M	07:20 AM	1.5	46
	01:43 PM	1.1	34
	05:02 PM	1.2	37
21 Tu	12:32 AM	0.1	3
	08:46 AM	1.5	46
	02:52 PM	1.2	37
	05:19 PM	1.2	37
22 W	01:18 AM	0.1	3
	10:00 AM	1.5	46
23 Th	02:12 AM	0.2	6
	11:06 AM	1.5	46
24 F	03:12 AM	0.3	9
	12:18 PM	1.4	43
25 Sa ◐	04:15 AM	0.4	12
	01:17 PM	1.4	43
26 Su	05:36 AM	0.6	18
	01:53 PM	1.3	40
	08:29 PM	1.0	30
	11:12 PM	1.0	30
27 M	06:58 AM	0.7	21
	02:17 PM	1.2	37
	08:26 PM	0.9	27
28 Tu	01:07 AM	1.1	34
	07:54 AM	0.7	21
	02:27 PM	1.2	37
	08:46 PM	0.8	24
29 W	02:23 AM	1.1	34
	08:42 AM	0.8	24
	02:27 PM	1.2	37
	09:13 PM	0.7	21
30 Th	03:28 AM	1.2	37
	09:32 AM	0.9	27
	02:39 PM	1.2	37
	09:43 PM	0.6	18

May

	Time	Height (ft)	Height (cm)
1 F	04:27 AM	1.3	40
	10:29 AM	1.0	30
	02:57 PM	1.2	37
	10:14 PM	0.5	15
2 Sa	05:13 AM	1.3	40
	11:22 AM	1.0	30
	03:13 PM	1.2	37
	10:44 PM	0.4	12
3 Su	05:50 AM	1.4	43
	12:09 PM	1.1	34
	03:19 PM	1.2	37
	11:11 PM	0.3	9
4 M ○	06:28 AM	1.4	43
	12:57 PM	1.1	34
	03:22 PM	1.2	37
	11:37 PM	0.3	9
5 Tu	07:13 AM	1.5	46
6 W	12:06 AM	0.2	6
	08:17 AM	1.5	46
7 Th	12:39 AM	0.2	6
	09:30 AM	1.5	46
8 F	01:20 AM	0.2	6
	10:23 AM	1.5	46
9 Sa	02:10 AM	0.2	6
	11:11 AM	1.5	46
10 Su	03:07 AM	0.3	9
	11:54 AM	1.4	43
11 M ◑	04:08 AM	0.4	12
	12:22 PM	1.3	40
	07:37 PM	1.0	30
	10:02 PM	1.0	30
12 Tu	05:37 AM	0.6	18
	12:45 PM	1.3	40
	07:49 PM	0.9	27
13 W	12:33 AM	1.1	34
	07:25 AM	0.7	21
	01:10 PM	1.2	37
	08:14 PM	0.7	21
14 Th	02:12 AM	1.2	37
	08:31 AM	0.8	24
	01:37 PM	1.2	37
	08:44 PM	0.5	15
15 F	03:38 AM	1.3	40
	09:39 AM	1.0	30
	02:04 PM	1.2	37
	09:21 PM	0.3	9
16 Sa	04:56 AM	1.4	43
	10:50 AM	1.1	34
	02:32 PM	1.2	37
	10:05 PM	0.1	3
17 Su	05:52 AM	1.5	46
	11:51 AM	1.1	34
	02:59 PM	1.2	37
	10:50 PM	0.0	0
18 M ●	06:44 AM	1.6	49
	12:45 PM	1.2	37
	03:25 PM	1.3	40
	11:33 PM	0.0	0
19 Tu	07:43 AM	1.6	49
	01:41 PM	1.2	37
	03:51 PM	1.3	40
20 W	12:13 AM	0.0	0
	08:50 AM	1.5	46
21 Th	12:52 AM	0.1	3
	09:46 AM	1.5	46
22 F	01:34 AM	0.2	6
	10:33 AM	1.4	43
23 Sa	02:21 AM	0.3	9
	11:18 AM	1.3	40
24 Su	03:10 AM	0.5	15
	12:01 PM	1.3	40
25 M ◐	03:56 AM	0.6	18
	12:32 PM	1.2	37
	07:33 PM	0.8	24
	11:07 PM	0.9	27
26 Tu	05:44 AM	0.7	21
	12:45 PM	1.2	37
	07:47 PM	0.7	21
27 W	01:36 AM	1.0	30
	07:16 AM	0.8	24
	12:56 PM	1.1	34
	08:12 PM	0.6	18
28 Th	02:52 AM	1.0	30
	08:10 AM	0.9	27
	01:13 PM	1.1	34
	08:39 PM	0.5	15
29 F	04:00 AM	1.1	34
	09:01 AM	1.0	30
	01:31 PM	1.1	34
	09:08 PM	0.3	9
30 Sa	04:54 AM	1.2	37
	10:07 AM	1.0	30
	01:43 PM	1.1	34
	09:39 PM	0.2	6
31 Su	05:34 AM	1.3	40
	11:15 AM	1.1	34
	01:41 PM	1.1	34
	10:09 PM	0.1	3

June

	Time	Height (ft)	Height (cm)
1 M	06:08 AM	1.3	40
	10:41 PM	0.1	3
2 Tu ○	06:43 AM	1.4	43
	11:13 PM	0.0	0
3 W	07:25 AM	1.4	43
	11:46 PM	-0.1	-3
4 Th	08:24 AM	1.4	43
5 F	12:22 AM	0.0	0
	09:18 AM	1.4	43
6 Sa	01:02 AM	0.0	0
	09:54 AM	1.3	40
7 Su	01:50 AM	0.1	3
	10:20 AM	1.3	40
8 M	02:46 AM	0.3	9
	10:44 AM	1.2	37
9 Tu ◑	03:47 AM	0.5	15
	11:10 AM	1.2	37
	06:43 PM	0.7	21
	11:11 PM	0.9	27
10 W	05:32 AM	0.6	18
	11:39 AM	1.1	34
	07:17 PM	0.5	15
11 Th	01:48 AM	1.0	30
	07:24 AM	0.8	24
	12:10 PM	1.1	34
	07:52 PM	0.3	9
12 F	03:17 AM	1.1	34
	08:30 AM	0.9	27
	12:41 PM	1.1	34
	08:28 PM	0.1	3
13 Sa	04:32 AM	1.2	37
	09:37 AM	1.0	30
	01:11 PM	1.1	34
	09:08 PM	-0.1	-3
14 Su	05:27 AM	1.3	40
	10:50 AM	1.1	34
	01:38 PM	1.1	34
	09:51 PM	-0.1	-3
15 M	06:12 AM	1.4	43
	11:48 AM	1.1	34
	02:03 PM	1.2	37
	10:37 PM	-0.2	-6
16 Tu ●	06:56 AM	1.4	43
	11:19 PM	-0.2	-6
17 W	07:45 AM	1.3	40
	11:57 PM	-0.1	-3
18 Th	08:37 AM	1.3	40
19 F	12:31 AM	0.0	0
	09:22 AM	1.2	37
20 Sa	01:03 AM	0.1	3
	09:55 AM	1.2	37
21 Su	01:36 AM	0.2	6
	10:20 AM	1.1	34
22 M	02:12 AM	0.4	12
	10:37 AM	1.1	34
	05:31 PM	0.7	21
	09:09 PM	0.8	24
23 Tu	02:52 AM	0.5	15
	10:55 AM	1.0	30
	06:25 PM	0.6	18
	10:58 PM	0.7	21
24 W ◐	03:31 AM	0.6	18
	11:18 AM	1.0	30
	07:04 PM	0.5	15
25 Th	01:49 AM	0.8	24
	04:11 AM	0.8	24
	11:43 AM	1.0	30
	07:36 PM	0.3	9
26 F	02:57 AM	0.9	27
	07:45 AM	0.9	27
	12:07 PM	1.0	30
	08:06 PM	0.2	6
27 Sa	04:01 AM	1.0	30
	08:38 AM	0.9	27
	12:18 PM	1.0	30
	08:36 PM	0.1	3
28 Su	04:52 AM	1.1	34
	09:39 AM	1.0	30
	12:07 PM	1.0	30
	09:05 PM	0.0	0
29 M	05:30 AM	1.2	37
	09:37 PM	-0.1	-3
30 Tu	06:03 AM	1.2	37
	10:13 PM	-0.2	-6

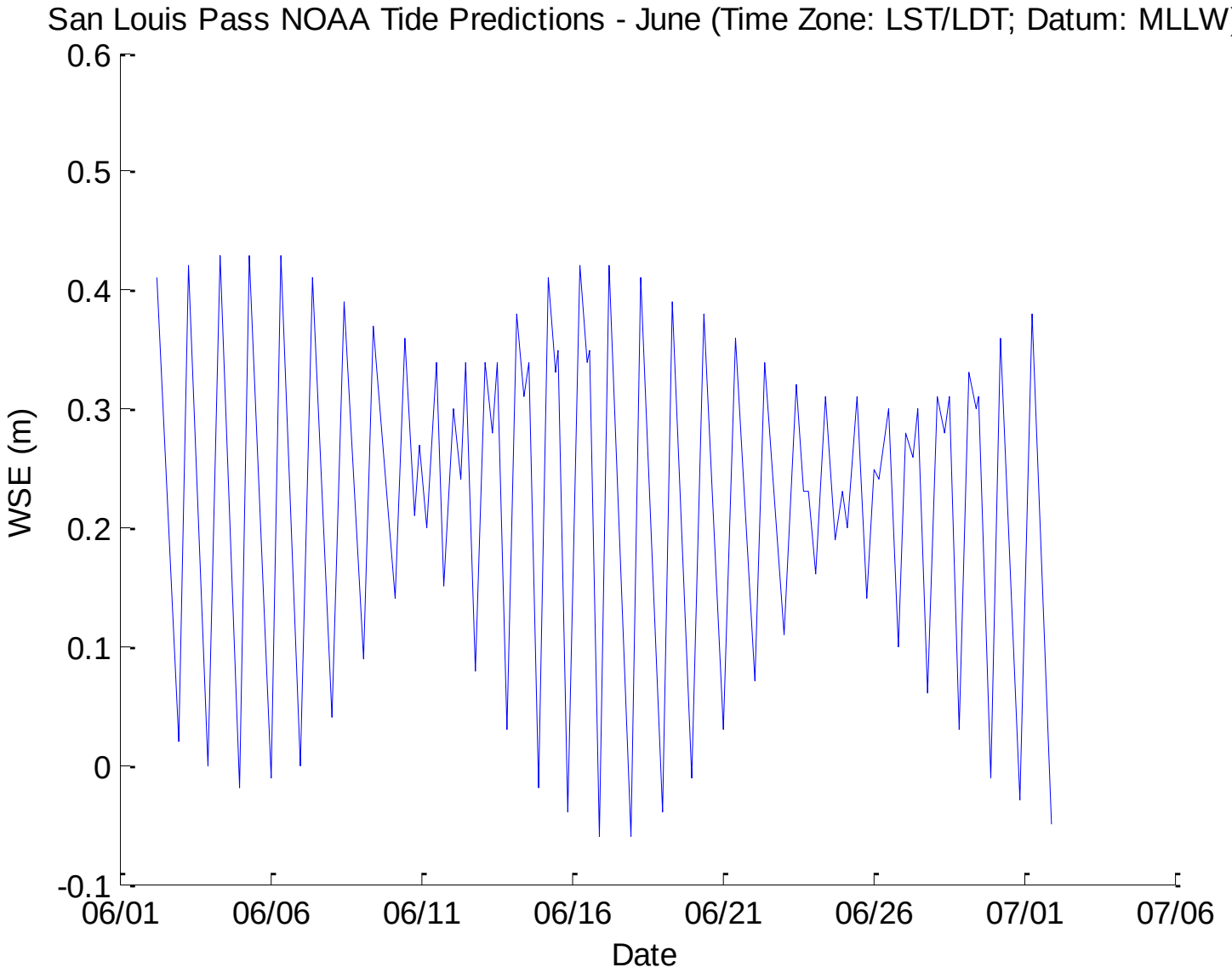
San Louis Pass NOAA Tide Predictions - June (Time Zone: LST/LDT; Datum: MLLW)
WSE (m)
0.6
0.5
0.4
0.3
0.2
0.1
0
-0.1
06/01
06/06
06/11
06/16
06/21
06/26
07/01
07/06
Date

Equipment Setup

Boat

- 2 boats will be for the deployment: the PARKER 25 for the offshore, kayaks will be used for the bay deployment
- The Parker will be located at Freeport Docks which Josh will navigate to
- The kayaks will be received en route to the deployment at Tim Dellapenna's house

Battery installation

Aquadopps

- All parts necessary are located in PMEC 244
- Aquadopps and Aquadopp batteries are located in blue Nortek cases
- Uncrew cap from bottom end
- Insert battery and plug in
- Apply thin layer of waterproofing gel to O-ring (gel is in the small plastic box inside of the Blue Nortek Aquadopp cases)
- Screw cap back on

Aquadopp Battery Cannisters

- All parts necessary are located in PMEC 244
- External canisters are located in large black box
- Unscrew cap
- Insert and plug in long battery located on the bottom shelf of the bookcase
- Apply thin layer of waterproofing gel to O-ring (gel is in the small plastic box inside of the Blue Nortek Aquadopp cases)
- Screw cap back on

Pingers

- All parts necessary are located in PMEC 244
- Unscrew plastic ring under the transducers
- Gently pull on the ring to expose board and batty mounts
- Install 6 9-volt batteries into each pinger (The batteries are in a plastic bag in the black box)

- The settings should already be set but if not use paper guide found inside pinger
    - Power output set at .5 watts
    - Rep rate set at 2 seconds in between reps
    - Power activation set for Water
    - Pulse length set to 2 ms
- Replace the board with batteries and screw back together

Mount Configuration

- The Aquadopp mounts are comprised of two main leg components which are bolted together to create a cross which the Aquadopp can be secured to.
- Insert bolts through both legs in the predrilled holes secure with washers, lock washers, and nuts (Hardware is located in one of the Aquadopp cases)
- Aquadopp will sit on top of raised U-channel and secured with hose clamps
- OBS will be mounted with hose clamps near head of Aquadopp
- Battery pack will be secured to one arm of mount with hose clamps
- Pinger will be secured to handle of mount with rope

Compass Calibration

- **Aquadopp will be fully mounted in an open area away from metal**
- Connect Squadopp to Dell Laptop found in PMEC 244
- Open AquaproHR program
- Connect the Aquadopp to the program
- Select the compass calibration located in the on-line tab
- Follow program directions

Time zone, coordinates, units, datum

Use CDT for for ALL (imagers, data loggers, and site photos, etc.)

All processed "final" data will be reported in these units. Attempt to collect all raw data using these values. If other values must be used, explicit notation should be made in the instrument log.

Parameter	Value
Date/time datum	Central Daylight Time (CDT)
Folder naming	yyyymmdd
File naming	InsID_yyyymmdd_hhmmEDT (start time) ("InsID" is the instrument ID) (Start time is 6/10/2015 12:00AM CDT)
Date/time format (for analysis)	MATLAB datenum (number of days since January 1, 0000 EDT)
Orthometric elevation datum	NAVD88
Ellipsoid and horizontal datums	NAD83
Projection and coordinate system	UTM 18 N
Units for orthometric elevation, ellipsoid height, horizontal coordinates and all lengths/distances	Meters
Relative elevations	Meters above or below a specified hard measuring point that will be surveyed (the sediment is not a measuring point)

Table C.2 Key Parameters

Time Sync

- Nortek Aquadopp programs will set the internal clocks (OBS piggyback off of other instrument clock) using Dell Laptop
- All dates and times should be set to the correct time in CDT

- **TIME SYNC COMPUTER BEFORE SYNCING INSTRUMENTS**

Measuring Scheme

- Aquadopps will be set to record in burst samples
- The burst interval will be set to 600 s
- 1024 samples per burst at 2 Hz rate using all three beams
- Sampling scheme outputs are copied below